Perspectives on Dye Sensitization of Nanocrystalline Mesoporous Thin Films

Ke Hu, Renato N. Sampaio, Jenny Schneider, Ludovic Troian-Gautier, and Gerald J. Meyer*

Department of Chemistry, University of North Carolina at Chapel Hill,

Chapel Hill, North Carolina, 27599-3290, United States

*Corresponding Author. gjmeyer@email.unc.edu

ABSTRACT. Recent advances in our mechanistic understanding of dye-sensitized electron transfer reactions occurring at metal oxide interfaces are described. These advances were enabled by the advent of mesoporous thin films, comprised of anatase TiO_2 nanocrystallites, that are amenable to spectroscopic and electrochemical characterization in unprecedented molecular-level detail. The metal-to-ligand charge transfer (MLCT) excited states of Ru polypyridyl compounds serve as the dye-sensitizers. Excited-state injection often occurs on ultrafast timescales with yields that can be tuned from unity to near zero through modification of the sensitizer or the electrolyte composition. Transport of the injected electron and the oxidized sensitizer (hole-hopping) are both operative in the composite mechanism for charge recombination between the injected electron and the oxidized sensitizer. Sensitizers that contain a pendant electron donor, as well as core/shell TiO_2/SnO_2 nanostructures, often prolong the lifetime of the injected electron and provide fundamental insights into adiabatic and non-adiabatic electron transfer mechanisms. Regeneration of the oxidized sensitizer by iodide is enhanced through halogen bonding, orbital pathways, and ion-pairing. A substantial ~ 10 MV cm^{-1} electric field is created by electron injection into TiO_2 nanocrystallites that induces ion migration, reports on the sensitizer dipole orientation, and (in some cases) re-orients or flips the sensitizer. Dye-sensitized conductive oxides also promote long-lived charge separation with bias dependent kinetics that provide insights into the reorganization energies associated with electron and proton-coupled electron transfer in the electric double layer.

Introduction

Early dye-sensitization research focused on silver halide reduction for latent image formation applications in photography.[1] Photoelectrochemists in the 1960s, in particular the late Heinz Gerischer, sensitized planar metal oxide materials to test and develop theories for interfacial electron transfer.[2-4] Dye sensitization of colloidal semiconductor suspensions explored throughout the 1980s was inspired by possible applications in solar water splitting.[5] O'Regan and Grätzel reported a substantial breakthrough in solar-to-electrical energy conversion with the advent of mesoporous thin (4-6 μm) films comprised of inter-connected anatase TiO_2 nanocrystallites (20 nm diameter) , **Figure 1a**.[6] The light-to-electrical energy conversion realized in regenerative solar cells based on these materials marked the first time that the performance of a molecular light absorber was at all comparable to solid-state photovoltaic materials.[7,8] More relevant to this Perspective article is the fact that these mesoporous thin films allowed spectroscopic *and* electrochemical characterization of interfacial electron transfer processes in molecular level detail that was not previously possible.

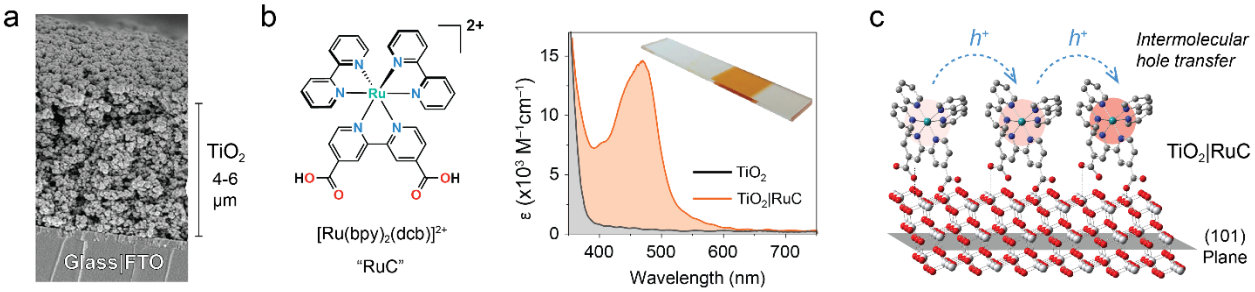

Figure 1. a) A plan SEM view of a mesoporous nanocrystalline (anatase) TiO_2 thin film on a fluorine-doped tin oxide glass substrate, b) the molecular structure of $[Ru(bpy)_2(dcb)]^{2+}$, abbreviated RuC and the absorption spectra of TiO_2 and TiO_2|RuC, and c) lateral intermolecular self-exchange "hole hopping" across the TiO_2 surface.

The metal-to-ligand charge-transfer (MLCT) excited states of $(d\pi)^6$ coordination compounds (sensitizers) continue to be the most optimal for fundamental study of photoinduced electron transfer reactions.[9] Surface coverages on the order of 10^{-8} mol cm^{-2} are realized when $[Ru(bpy)_3]^{2+}$, where bpy is 2,2'-bipyridine, sensitizers with carboxylic or phosphonic acid groups are reacted with a mesoporous thin film.[7,8] This corresponds to about a thousand fold increase in surface area relative to a planar electrode and a tremendous improvement in the solar light harvesting efficiency. About 500 sensitizers are present on each TiO_2 nanocrystallite, consistent with that expected for a molecular monolayer. The close proximity of the sensitizers enables lateral intermolecular energy and electron transfer 'hole hopping' reactivity, **Figure 1c**.

Of particular importance to this Perspective are the kinetics for excited-state electron injection and recombination of the injected electron with the oxidized sensitizer. These interfacial electron transfer reactions are understood with the Gerischer type diagram shown in **Figure 2**.[2-4] Excited-

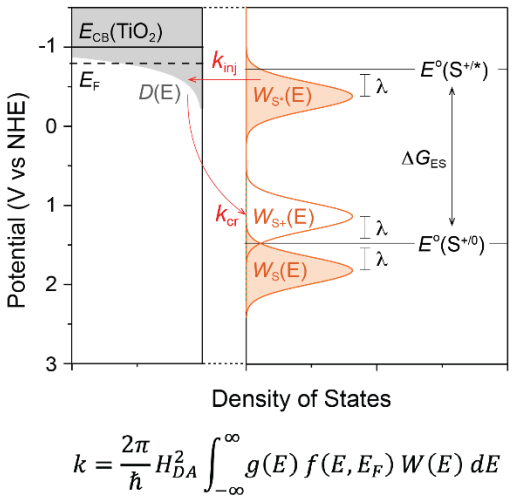

Figure 2. A Gerischer diagram relevant to excited-state injection and charge recombination.

state injection occurs from a Gaussian distribution of sensitizer donor states located below the excited-state potential $E°(S^{+/*})$ + λ, where λ is the total reorganization energy. Recombination occurs from the conduction band edge E_{CB}, to the oxidized sensitizer distribution. Gerischer emphasized that an interfacial rate constant, *k,* was related to the integrated overlap of the molecular distributions *W*(E) with the semiconductor *D*(E) and the product of the electronic coupling, H_{DA}, squared. Such diagrams accurately predict activationless electron injection when $E°(S^{+/*})$ is greater than 2λ above E_{CB}, and slow recombination when $E°(S^{+/0})$ lies within the forbidden energy gap. Note that in mesoporous nanocrystalline materials the nature of the redox active states as conduction band or localized $Ti^{IV/III}$ states remains contentious.[7,8] It is also interesting to note that λ is expected to be highly sensitive to the sensitizer location within the electric double layer, a point which is detailed in Section D.

The primary goal of this Perspective article is to provide our state-of-the-art mechanistic understanding of dye-sensitized interfacial molecular reactions in mesoporous anatase TiO_2 thin films in acetonitrile and aqueous electrolytes. Some specific questions that this Perspective hopes to address include:

- What mechanistic insights on interfacial electron transfer have been garnered since Gratzel and O'Regan's 1991 breakthrough?
- What key unanswered questions remain in dye-sensitization?
- What might be learned by utilizing oxides other than anatase TiO_2?
- What applications might be enabled by further mechanistic study of dye-sensitization?

Discussion and Perspectives

A. Excited-state Electron Transfer.

i. Excited-State Injection Kinetics. A significant advance in excited-state injection was garnered from study of a dozen $[Ru^{II}(4,4'\text{-}(PO_3H_2)_2\text{-bpy})(LL)_2]^{2+}$ sensitizers, where (LL) is an ancillary bpy ligand used to tune the excited-state potentials from −0.69 to −1.03 V vs NHE, **Figure 3a**.[10] Note that a common reference sensitizer in this Perspective is (LL) = bpy, abbreviated as TiO_2|RuP. Excited-state injection showed biphasic kinetics occurring mainly on the 3–30 ps and 30–500 ps range in acidic aqueous solution, **Figure 3b**. The slower process was assigned to injection from the luminescent ^{3}MLCT excited state. In agreement with Gerischer theory,[3] the rate constants were directly correlated with the energetic overlap of the TiO_2 acceptor states and the excited-state $E^o(Ru^{III/II*})$. The faster components were assigned to injection from higher energy excited states. The data indicate that the commonly reported non-exponential injection kinetics can simply be attributed to a continuous decrease in the injection rate constants that accompanies excited-state relaxation from the initially formed Franck-Condon state to the thermally equilibrated ^{3}MLCT state, **Figure 3b**.

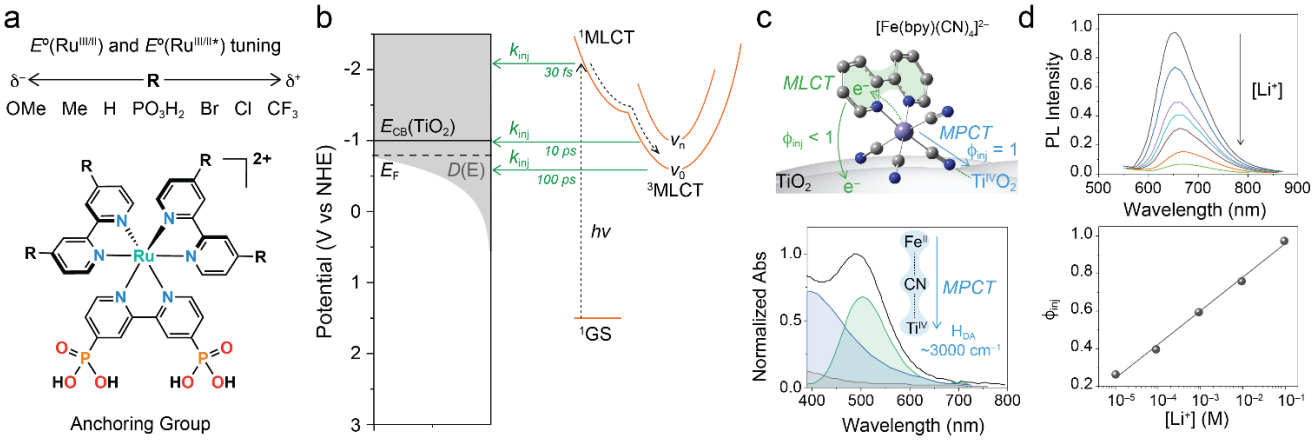

Figure 3. a) Structure of Ru^{II} sensitizers , when R=H the sensitized materials are abbreviated as TiO_2|RuP. b) Excited state electron injection from ^{1}MLCT and thermally-equilibrated ^{3}MLCT states. c) Metal-to-ligand (MLCT) and metal-to-particle (MPCT) excited state injection from $[Fe(bpy)(CN)_4]^{2-}$. d) Photoluminescence quenching of TiO_2|RuC by the Li^+ in CH_3CN that is correlated with the excited-state injection quantum yield.

The success of ruthenium based sensitizers and observation of ultrafast injection has motivated its replacement by iron. Due to their very short MLCT excited-state lifetimes, Fe^{II} diimine complexes typically display small injection yields with spectroscopic features characteristic of high spin ligand field states; injection is kinetically slow relative to intersystem crossing and/or

internal conversion.[14-17] A recent break through was the discovery that N-heterocyclic Fe^{II} complexes provide greatly enhanced injection yields, $\phi_{inj} > 0.9$.[18-22] This exciting advance appears to emanate from much longer-lived MLCT excited states and may soon enable efficient energy conversion with a first row transition metal sensitizer. Excited-state injection yields near unity have also been reported for Co^{I} complexes, including Vitamin B_{12}.[23] An intriguing aspect of this interfacial chemistry is that the initial Co^{I} state is 4-coordinate, while the Co^{II} product adopts a 5-coordinate geometry. Hence the coordination number changes that accompany $Co^{II/I}$ redox chemistry provides an opportunity to control the reaction.[23]

Alternative pathways exist for the transfer of electrons from sensitizers to TiO_2 with light. For sensitizers linked to TiO_2 through ambidentate cyanide ligands, metal-to-particle Fe^{II}-CN-Ti^{IV} → Fe^{III}-CN-Ti^{III} charge transfer (MPCT) absorption band are evident.[24-28] An advantage of MPCT is that quantitative injection yields are realized. Indeed, in a series of TiO_2|$Fe(CN)_4$(LL) ϕ_{inj} was 1 for MPCT while injection from the MLCT state was inefficient and ionic strength dependent.[25] A mechanistic advantage of MPCT transitions is that they are amenable to Mulliken-Hush analysis, providing estimates of H_{DA} and λ. An $H_{DA} \sim 3000$ cm^{-1} was reported, a value in good agreement with known mixed-valent metal cyanide complexes and subsequent analysis through Stark spectroscopy.[26,27] The spectral breadth of the MPCT transition provides large reorganization energies that DFT calculations suggest is due to a localized $Ti^{IV/III}$ redox reaction that is expected to be subject to a Jahn-Teller distortion.[28]

ii. Influence of pH. It is well known in the photoelectrochemical literature that the surface adsorption of electrolyte cations can induce dramatic shifts in the energetic positions of the valence and conduction band edges while maintaining a constant band gap, *i.e.* the band edges move in parallel.[29] The classical example is the Nernstian 59 mV/pH shift of the band edges, that is generally attributed to the equilibrium shown in **equations 1 and 2**.[30,31] For anatase TiO_2 this acid-base equilibria is not necessarily confined to the surface and may also occur within the crystalline lattice.[31]

$$Ti^{IV}OH_2^+ \rightleftharpoons Ti^{IV}OH + H^+ \qquad (1)$$

$$Ti^{IV}OH \rightleftharpoons Ti^{IV}O^- + H^+ \qquad (2)$$

Sutin reported a strong pH dependence to dye-sensitized photocurrents with rutile TiO_2 single crystals.[32] Assuming a Nernstian shift of E_{CB}, the reorganization energy was estimated to be λ = 0.25 eV. A curious aspect of this early work was a noted discrepancy between the predicted and measured pH onset. Watson and coworkers re-investigated this with four porphyrins, whose excited-state reduction potentials spanned a 660 mV range.[33] Interestingly, the pH onset was sensitizer independent and considerably more acidic than expected. A mechanism was proposed

wherein excited-state injection occurred from pH 12 to 2, yet a sustained photocurrent required protonation of a surface Ti(III) titanol group that only occurred at pH < 3. Hence, the pH dependent photocurrents reflected the charge collection efficiency and not the excited-state injection yield. There remains little precedence for such geminate recombination in the dye-sensitized TiO_2 literature and this interesting behavior deserves further experimental work.[7,26]

iii. Influence of Electrolyte Cations in Organic Solvents. Reduction of anatase TiO_2 results in the appearance of a well-documented blue-black color.[29,34] The spectrum is insensitive to the identity of the electrolyte, but the potential onset for coloration is not. Reduction occurs at applied potentials almost 1 eV more positive in Li^+ than TBA^+ CH_3CN electrolytes, where TBA is tetrabutylammonium.[34-37] Li^+ is hence considered a 'potential determining ions' as are other alkali and alkaline earth cations. It appears that the commercially available and sol-gel processed anatase TiO_2 thin films preferentially adsorb cations from organic solutions. Note that in water, the coloration onset potential is determined solely by the proton concentration, 59 mV/pH.[29-31]

Based on these energetics, one would anticipate inefficient excited-state injection unless a potential determining cation was present in the CH_3CN electrolyte. Indeed, light excitation of $[Ru^{II}(4,4'\text{-}(CO_2H)_2\text{-bpy})(bpy)_2]^{2+}$, abbreviated TiO_2|RuC in neat CH_3CN resulted in long-lived excited states with $\phi_{inj} < 0.2$. The yields increased to unity when Li^+, or other alkali or alkaline-earth cations were present in the CH_3CN.[34] It was possible to reversibly tune ϕ_{inj} from near zero to unity just by controlling the Li^+ concentration in the external acetonitrile solution, **Figure 3d**. A correlation of ϕ_{inj} with the size-to-charge ratio of the cations suggested that Lewis acid-base interactions with the oxide lowered the $Ti^{IV/III}$ reduction potential resulting in better energetic overlap with the excited state sensitizer levels. An alternative explanation is that adsorbed cations stabilize surface hydroxide ions and decrease the interfacial pH. Indeed the presence of strong Lewis acids or protons in the electrolyte often results in desorption of the protonated from of the sensitizer.[34,38] An energetic shift of the TiO_2 acceptor states with electrolyte cation provides a simple explanation for O'Regan and Gratzel's observation that the photocurrent was larger (and the open circuit photovoltage smaller) when LiI was utilized instead of TBAI.[6]

Decoupling the TiO_2 band edge positions from the electrolyte composition is beneficial to some solar applications. Toward this goal, Morris and coworkers utilized surface functionalization, with long alkyl chains that contain a terminal alkoxysiloxane, phosphonate, or carboxylic acid group, as a means to control cation adsorption.[39] In the absence of a potential determining cation, surface functionalization lowered the energy of the acceptor states, *i.e.* shifted them away from the vacuum level. When $LiClO_4$ was present in the electrolyte, the TiO_2 reduction onset was not affected, but the density of states at more negative potentials decreased significantly suggesting that the surface functionalization did indeed inhibit Li^+ adsorption.

B. Sensitizer Regeneration.

The iodide/iodine redox mediator has been the subject of several prior reviews and will only be summarized here.[40,41] For champion sensitizers, iodide oxidation occurs on a hundred of nanosecond time scale. Incident-photon-to-current efficiencies (IPCE) measured at the short circuit condition often indicated that both excited state injection and regeneration occur with a quantum yield of one. However, regeneration is not quantitative at the open circuit or power point conditions[42,43] because recombination is much more rapid when the number of electrons in each nanocrystallite is large.[44] It is not sufficient for S^+ to be thermodynamically competent of iodide oxidation, the reaction must occur more rapidly than the competitive recombination reaction. The realization that regeneration can be further optimized continues to inspire research to design interfaces capable of more efficient iodide oxidation.

i. Halogen and Chalcogen Bonding. A successful approach for enhancing regeneration was realized with sensitizers capable of halogen and chalcogen bonding **Figure 4**.[45-49] In collaboration with the Berlinguette group, a series of four D-π-A sensitizers were investigated with triphenylamine donors bearing halogen atoms in the para-position of the two terminal phenyl rings, **Figure 4b**.[46] DFT calculations revealed a significant σ-hole for the oxidized forms of the iodo- and bromo- sensitizers yet not for the fluoro-sensitizer, results consistent with the larger halogen bonding field.[49-51] Kinetic studies revealed a correlation between the sensitizer's ability to halogen bond and the 2nd order rate constant for iodide oxidation. Synchrotron studies provided direct evidence for a nucleophile-σ-hole adduct.[47] While the enhancements in the power conversion efficiency were small, these studies provided a proof-of-principle demonstration that halogen bonding can be quantified and utilized to enhance electron transfer kinetics at molecular-semiconductor interfaces.

The observation of halogen bonding raised the more general question of whether iodide oxidation takes place by inner- or outer sphere mechanisms.[52,53] In other words, does iodide form a bond with the oxidized sensitizer prior to electron transfer? To address this question, a series of five sensitizers with a heterocyclic group competent of forming a chalcogen-iodide bond were investigated.[48] The free energy change for regeneration was small and core/shell SnO_2/TiO_2, materials enabled iodide oxidation to compete kinetically with recombination. Under such conditions, the collisional frequency was large thereby magnifying the desired intermolecular interactions. Indeed, more rapid iodide oxidation was evident when the β-LUMO of the oxidized sensitizer had significant oxidizing character on the chalcogen atom, behavior attributed to enhanced electronic coupling through an inner-sphere orbital pathway.[48] This finding motivates the design of next generation sensitizers that have an orbital pathway for regeneration.

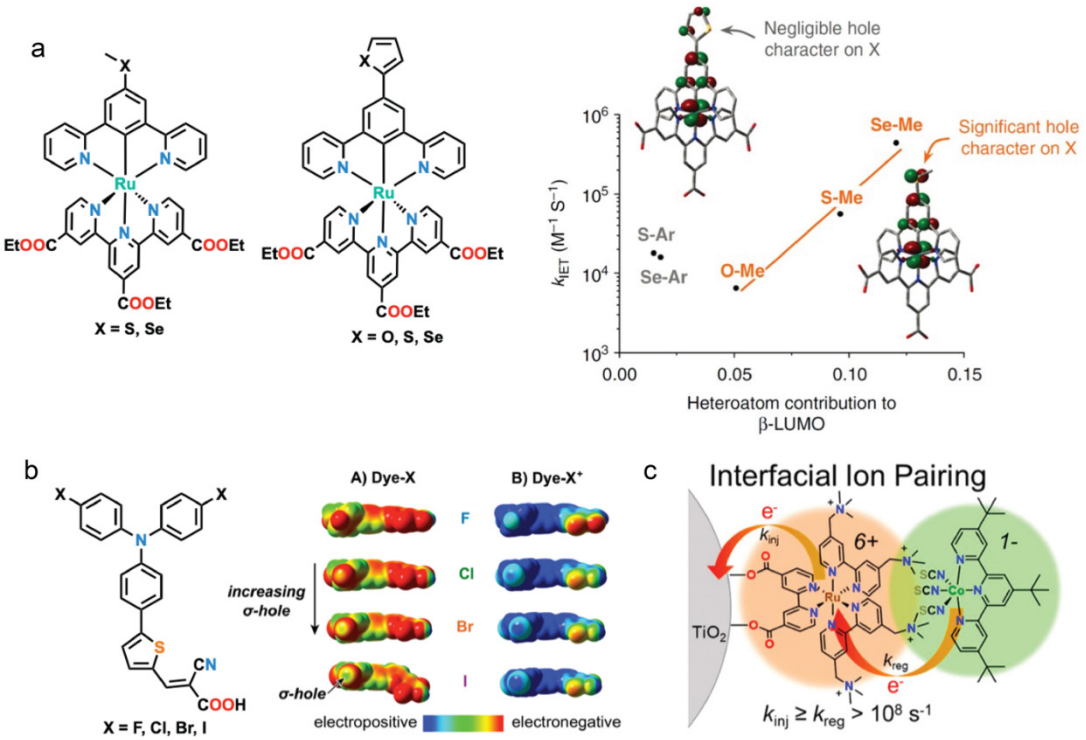

Figure 4. a) Sensitizers for chalcogen binding and a plot of the rate constant for iodide oxidation versus the chalcogen atom orbital contribution from the β-LUMO. b) Structure of the D-π-A sensitizers utilized for halogen bonding with DFT analysis showing that the σ-hole in the ground and oxidized states increases with the halogen principle quantum number. c) Representation of interfacial ion-pairing between surface anchored $[Ru(dcb)(tmam)_2]^{6+}$ and an anionic Co complex.

ii. Ion-Pairing. Many sensitizers are cationic in their ground and oxidized states,[40,41,53] yet until recently clear evidence of ion-pairing with iodide was lacking at dye-sensitized TiO_2 interfaces.[54] Highly cationic Ru(II) sensitizers, $[Ru(tmam)_2(dcb)]^{6+}$, where tmam is 4,4'-bis-(trimethylaminomethyl)-2,2'-bipyridine revealed clear evidence for ion-pairing with iodide as well as with an anionic cobalt redox mediator ($K_{eq} > 10^4$ M^{-1}) in CH_3CN, **Figure 4c**. With the Co mediators, excited-state injection *and* regeneration occurred on timescales less than 10 ns. Hence, the impact of ion-pairing was to remove the diffusional limitations generally associated with sensitizer regeneration. This ground-state association almost doubled the light-to-electrical energy conversion efficiency compared to cases where ion pairing was absent.[54] Hence highly charged cationic sensitizers undergo ion-pairing at dye-sensitized TiO_2 interfaces that promotes rapid regeneration.

C. Charge Recombination.

i. Slow Non-exponential, Concentration-Dependent Kinetics Recombination of an injected electron with an oxidized sensitizer yields ground-state products and typically wastes > 1 eV of free energy. Studies of TiO_2|RuC first revealed that charge recombination was not slow because

of inherently small rate constants, but rather because the process is second-order in nature.[34] Under conditions where the number of charge separated states was systematically varied, the same second-order rate constant was extracted. Excited-state injection creates one injected electron and one oxidized sensitizer and an overall second-order rate law r = $k[S^+][TiO_2(e^-)]$ might be anticipated.[55] While the numbers of injected electrons and oxidized sensitizers are equal, the concentrations implied by the brackets are quite different. Electrons are injected into a spherical nanocrystal interconnected to other nanocrystals in a mesoporous film while the oxidized sensitizers are confined to the quasi-two-dimensional surface. Thus recombination is a fascinating mechanistic process between redox equivalents on opposite sides of an interface with translational freedom that must first come into close proximity before exergonic electron transfer occurs.

While the second-order kinetic model adequately modelled recombination following light excitation of TiO_2|RuC, it did not provide adequate fits for gold standard sensitizers like N3, *cis*-$Ru(dcb)_2(NCS)_2$.[56] The widely utilized Kohlrausch-Williams-Watts (KWW) function, **equation 3**, is more generally applicable where k is the rate constant, A_0 is the initial amplitude, and β is inversely related to the width of an underlying Lévy distribution of rate constants $0 < \beta < 1$. An "average" rate constant, k_{cr}, can be calculated from the first moment, **equation 4**.[57,58]

$$A(t) = A_0 e^{-(kt)^\beta} \qquad (3)$$

$$k_{cr} = \frac{k\beta}{\Gamma\left(\frac{1}{\beta}\right)} \qquad (4)$$

An advantage of this function is that the normalized kinetic data are fit to only two parameters. Further, the inverse Laplace transform of this function is known at specific values of β and has been approximated at others, thereby providing the underlying Levy distribution, **Figure 5a**.[60] An unsatisfactory aspect is that such transformations are inherently ill-conditioned and the extracted KWW parameters are usually sensitive to the initial number of interfacial states that are photo-created. Hence meaningful comparative studies of different sensitizers require that initial concentrations of interfacial states be held constant.

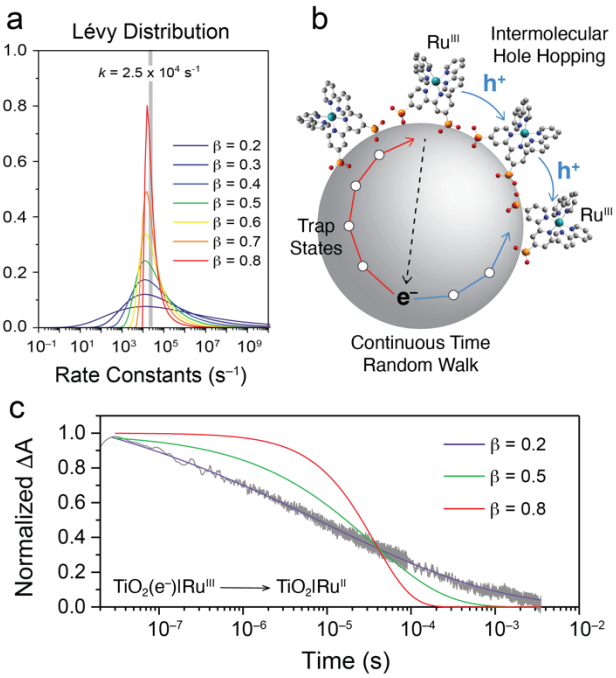

Figure 5. a) Lévy distribution of rate constants with k = 2.5 x 10^4 s^{-1} and the indicated β values. b) Illustration of injection electron, intermolecular self-exchange 'hole-hopping' and electron transport between trap states modelled as a continuous time random walk. c) Time resolved absorption change associated with $TiO_2(e^-)|Ru^{III} \rightarrow TiO_2|Ru^{II}$ charge recombination with overlaid fits to the KWW function, **Equation 3**.

ii. Kinetic Models and Hole-Hopping. The KWW function was proposed empirically by Kohlrausch and later derived by Scher and Montroll using a random walk kinetic model.[57-59] Nelson extended this model to dye-sensitized TiO_2 interfaces where the oxidized sensitizer remains fixed at the injection site and the injected electron undergoes thermally activated transport between traps states prior to recombination, **Figure 5b**.[61,62] Electron transport measurements have also revealed a significant light intensity dependence that may also be due to trapping.[63] The observed rate constants were hence expected to report on rate-limiting electron transport in the mesoporous thin film with fast interfacial electron transfer when the redox equivalents came in close proximity.

There are two aspects of the random-walk model that have not withstood the test of time. First, many comparative studies have shown that the rate constants are sensitive to the identity of the sensitizer and hence are not solely limited by electron transport.[64] Examples of this are given in the following section. Second, the oxidizing equivalent does not remain fixed at the injection site, but rather undergoes intermolecular self-exchange electron transfer with neighboring sensitizers that is often called 'hole hopping'.[65] The utilization of polarized light to create an anisotropic population of interfacial states has provided clear evidence that hole hopping follows excited-state injection under many experimental conditions.[66] Monte-Carlo simulations indicated that an oxidizing equivalent can circumnavigate the entire nanocrystal before charge recombination

occurs. [66,67] This remarkable result led to the conclusion that if properly controlled, hole-hopping could be utilized to transfer redox equivalents to desired locations. Mechanistic insights have also been garnered through electrochemical measurements wherein a potential step sufficient to oxidize the sensitizers initiates oxidation at the FTO substrate.[68,69] An advantage of the spectroscopic approach is that it is contactless and amenable to diverse experimental conditions. For example, hole-hopping is absent for TiO_2|RuC in neat CH_3CN, but rapid in 100 mM $LiClO_4/CH_3CN$; a finding that would be difficult to establish through electrochemical measurements alone.[66]

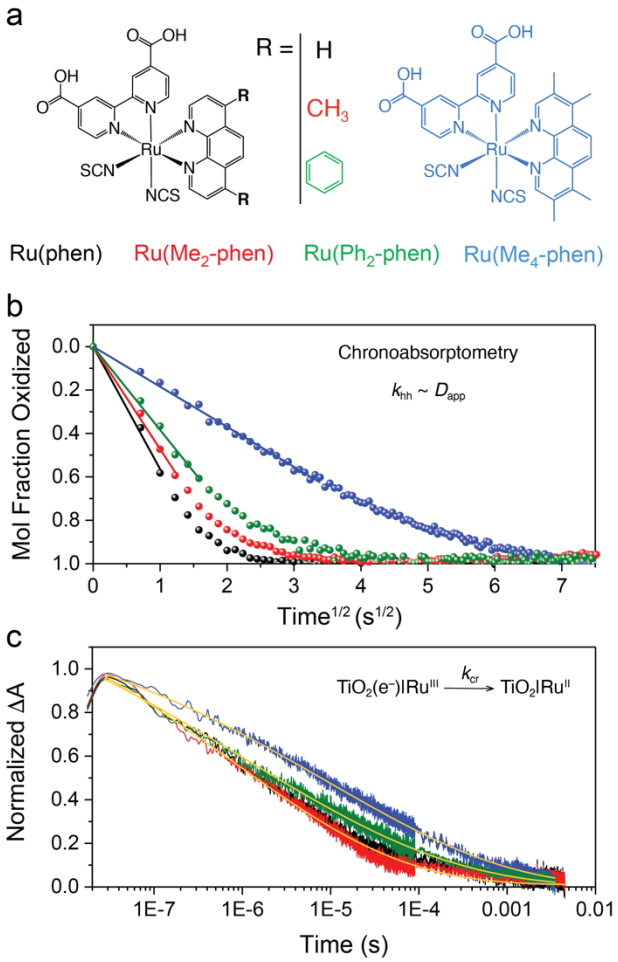

Figure 6. a) The *cis*-Ru(dcb)(phen')$(NCS)_2$ sensitizers utilized for hole hopping and charge recombination studies. The color code is used throughout this Figure. b) An Anson plot of the mole fraction of oxidized sensitizers plotted *vs.* $t^{1/2}$ measured after a potential step sufficient to oxidize the sensitizers. Overlaid is a fit from which the apparent diffusion coefficient, D_{app}, and hole-hopping rate constants, k_{hh}, were extracted. c) Normalized absorption changes due to $TiO_2(e^-)|Ru^{III} \rightarrow TiO_2|Ru^{II}$ charge recombination with overlaid fits to the KWW function.

An important mechanistic advance was the realization that hole-hopping rates are directly correlated with charge recombination.[70] Sensitizers that undergo fast hole-hopping recombine more rapidly than those that hop more slowly. This correlation was evident in a collaboration with

the Polo research group through a study of *cis*-Ru(dcb)(phen')$(NCS)_2$ sensitizers, where phen' is a 4,7-disubstituted 1,10-phenantholine, **Figure 6a**.[71-72] Chronoabsorptometry data, where the color change was monitored after a potential step sufficient to oxidize the sensitizers was applied, was recast as an Anson plot from the apparent diffusion constant, D_{app}, and the hole-hopping rate constant, k_{hh}, were extracted, **Figure 6b**. The k_{hh} values spanned about a factor of seven and followed the same trend as did charge recombination: Ru(Me_4-phen) << Ru(Ph_2-phen) < Ru(Me_2-phen) ~ Ru(phen). The correlation shown in **Figure 6** is not 1:1, yet provides strong evidence that lateral hole-hopping is mechanistically coupled to charge recombination.[72] The data also provide an alternative explanation for slow charge recombination with the classical N3 sensitizer, *cis*-$Ru(dcb)_2(NCS)_2$.[73] This sensitizer also displays unusually slow hole-hopping kinetics attributed to a surface orientation where one carboxylate group form each dcb ligand binds to the surface with decreased intermolecular electronic coupling relative to *cis*-Ru(dcb)(phen')$(NCS)_2$ sensitizers.[74] Temperature dependent kinetic studies made as a function of the surface coverage support the conclusion that rapid hole-hopping promotes charge recombination.[75] Taken together, these findings indicate that unwanted charge recombination can be inhibited through control of lateral hole-hopping, an unexpected finding that may be further exploited in future research.[76]

iii. Recombination to acceptor-bridge-donor (A-B-D) sensitizers. A proven strategy for inhibiting unwanted charge recombination is to regenerate the oxidized sensitizer by intramolecular electron transfer.[77-80] In this strategy, after excited-state injection the oxidizing equivalent (or 'hole') is transferred from the sensitizer to a donor by intramolecular electron transfer. Ideally intramolecular electron transfer is rapid and does not sacrifice much free energy. Early examples were used to boost the open circuit photovoltage of solar cells[80] and more recent studies have utilized water oxidation catalysts as the donors.[81] An interesting observation was that a relatively small structural change in the bridge altered the electron transfer mechanism from adiabatic to non-adiabatic. Interestingly, for adiabatic transfer there is no kinetic advantage to translation of the oxidizing equivalent or 'hole' away from the interface.[77]

Electron transfer theories predict that as the quantum mechanical mixing of the donor-and acceptor wavefunctions, H_{DA}, increases the absolute value of the free energy decreases, $|\Delta G^o_{ad}| < |\Delta G^o|$.[82-84] An increased H_{DA} is also expected to lower the electron transfer barrier. These theoretical expectations are difficult to test experimentally as formal reduction potentials are poor indicators of ΔG^o when H_{DA} is large.[85] To circumvent this difficulty, excited state injection into TiO_2 was utilized to initiate intramolecular electron transfer with kinetic analysis of the approach to equilibrium.[86] Four acceptor-bridge-donor (A-B-D) sensitizers were investigated where the bridge unit was designed to control H_{DA}.[86-88] Care was taken to ensure that the K_{eq} values were near unity so that a measurable concentration of all the species was present at equilibrium.

The sensitizers have two redox active groups that differ only by the orientation of an aromatic bridge that links them: a planar aromatic bridge (**p**) supports strong electronic coupling, H_{DA} > 1000 cm^{-1}; and a nonplanar (**x**) lowers the coupling, H_{DA} < 100 cm^{-1} without a significant change in the geometric distance.[87] **Figure 7** shows that substituents on the cyclometallating ligand tuned the $Ru^{III/II}$ reduction potential such that the free energy for hole transfer was unfavorable for **1,** and favorable for **2**.

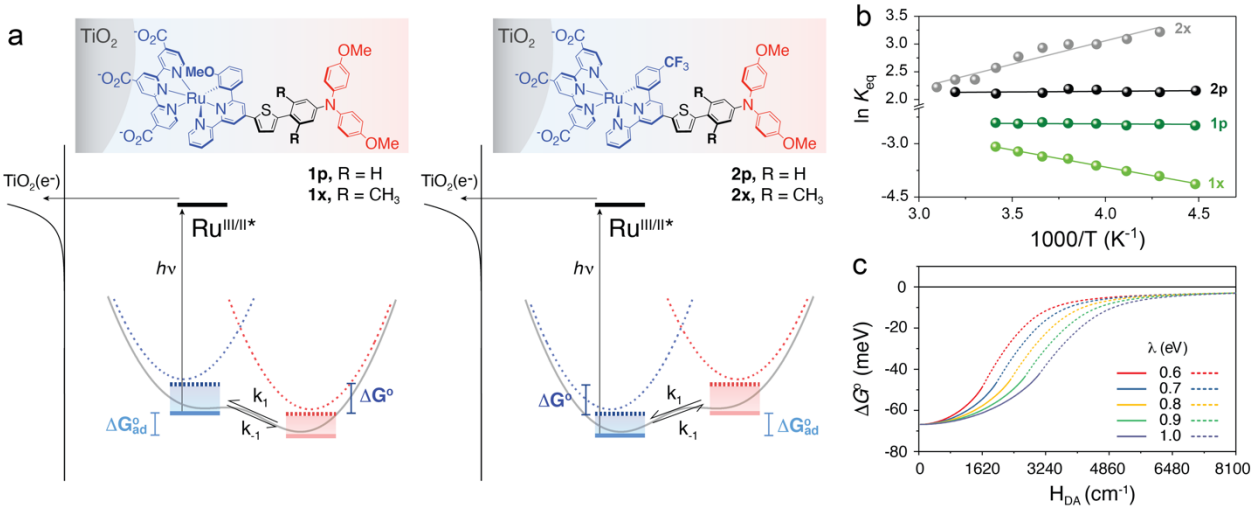

Figure 7. a) Structures of four Ru-B-TPA sensitizers that support adiabatic (**p**) and non-adiabatic (**x**) electron transfer. The potential energy surfaces show that after excited-state injection, intramolecular electron transfer from the remote TPA is disfavored for 1 and favored for 2. Note that the expectation of a smaller free energy change for adiabatic (solid) vs non-adiabatic (dashed) was realized experimentally while the corresponding decrease in the barrier was not (see text). b) A van't Hoff plot showing that the equilibrium constants for the **p** sensitizers were closer to unity than the **x**, consistent with $|\Delta G^{o}_{ad}| < |\Delta G^{o}|$. The data provide compelling evidence for an adiabatic equilibrium in the **p** sensitizers that is determined solely by ΔS^{o}. c) Plot of the Gibbs free energy change versus the electronic coupling for the indicated reorganization energies.

Pulsed light excitation resulted in a long-lived injected electron that provided sufficient time for a $Ru^{III/II}$-B-$TPA^{+/0}$ quasi-equilibrium to be established and for kinetic determination of the forward and reverse rate constants, $K_{eq} = k_1/k_{-1}$, over a 80° temperature range.[86] A significant kinetic barrier was measured under all conditions indicating that a true redox equilibrium was operative. A van't Hoff analysis provided clear evidence that K_{eq} was closer to unity for **p** and hence $|\Delta G^{o}_{ad}| < |\Delta G^{o}|$ as predicted theoretically, **Figure 7b**. The magnitude of the free energy loss from adiabatic electron transfer is significant and is a function of the reorganization energy, **Figure 7c**. Collectively the data show that the absolute magnitude of the thermodynamic driving force for electron transfers are decreased when adiabatic pathways are operative, a finding that should be considered in the design of hybrid materials for solar energy conversion. The data also provide a text book example of an adiabatic electron transfer equilibrium for the **p** sensitizers. This is significant since the classification as adiabatic, non-adiabatic or at the borderline is generally

unknown and often inferred from kinetic rate constants or by intuition. Here the van't Hoff data for the **p** sensitizers clearly indicate $\Delta H^o = q_p = 0$ providing an unambiguous case of adiabatic electron transfer. Adiabatic redox equilibrium constants are determined solely by ΔS^o. For the **x** sensitizers, $\Delta H^o = \pm 7.0$ kJ mol^{-1}and electron transfer is nonadiabatic.

A decreased electron transfer barrier is anticipated for adiabatic electron transfer. However, Eyring analysis revealed that $\Delta G^{\ddagger}$ was 30 kJ mol^{-1}for the uphill reaction and 25 kJ mol^{-1} for the downhill reaction regardless of the bridge identity.[88] The enthalpies of activation were in fact smaller for adiabatic electron transfer, but this was offset by a more unfavorable $\Delta S^{\ddagger}$. Hence this analysis supports an intriguing conclusion: while adiabaticity lowers $\Delta H^{\ddagger}$ for thermodynamically uphill reactions, $\Delta S^{\ddagger}$ becomes the dominant contributor to $\Delta G^{\ddagger}$. Because electron transfer in the **p** sensitizers satisfies criteria for solvent dynamical control, the impact of solvent and bridge motion (entropy) are expected to be critical. In contrast, **x** sensitizers lie within a nonadiabatic regime where electron transfer is limited by H_{DA}. Even though coupling accelerates electron transfer by allowing a rapid approach to the transition state, a substantial entropic penalty is imposed.[88] In addition, $\Delta S^{\ddagger}$ was shown to control interfacial electron transfer dynamics from anatase TiO_2 to molecular acceptors.[89] An unfavorable ΔS^o is also expected when an injected electron and an oxidized sensitizer with translational freedom localize on one sensitizer.

D. Interfacial Electric Fields.

Electrons injected into TiO_2 emanate an electric field that significantly influences the absorption spectra of surface anchored sensitizers.[90,91] The electro-absorption features provide a useful means to quantify the impact of electric fields on sensitizer orientation, ion migration (termed screening), and interfacial electron transfer.[92-105] The feature has also been utilized to quantify the field strength of rigid-rod sensitizers set at variable distances from the TiO_2 surface.[95] A simplified basis for the electro-absorption is shown in **Figure 8a**. A key parameter is the light induced dipole moment vector change, $\Delta\vec{\mu}$, of the sensitizer relative to the electric field vector, $\vec{E}$. A parallel orientation gives rise to a red shift in the absorption spectra and an anti-parallel orientation results in a blue shift, **Figure 8b**.[91,92] Interestingly, the surface adsorption of Lewis acidic cations induces spectral shifts in the opposite direction of those measured after excited state injection.[34] An example of the antiparallel orientation is given in **Figure 8c** for TiO_2|RuC.

In a single dipole approximation, the magnitude of the spectral shift, ΔU, reports directly on $\vec{E}$, **equation 6.** A more precise determination of $\vec{E}$ utilizes the first-derivative of the absorbance spectrum, **equation 7**.

$$\Delta U = -\Delta\vec{\mu} \cdot \vec{E} \qquad (6)$$

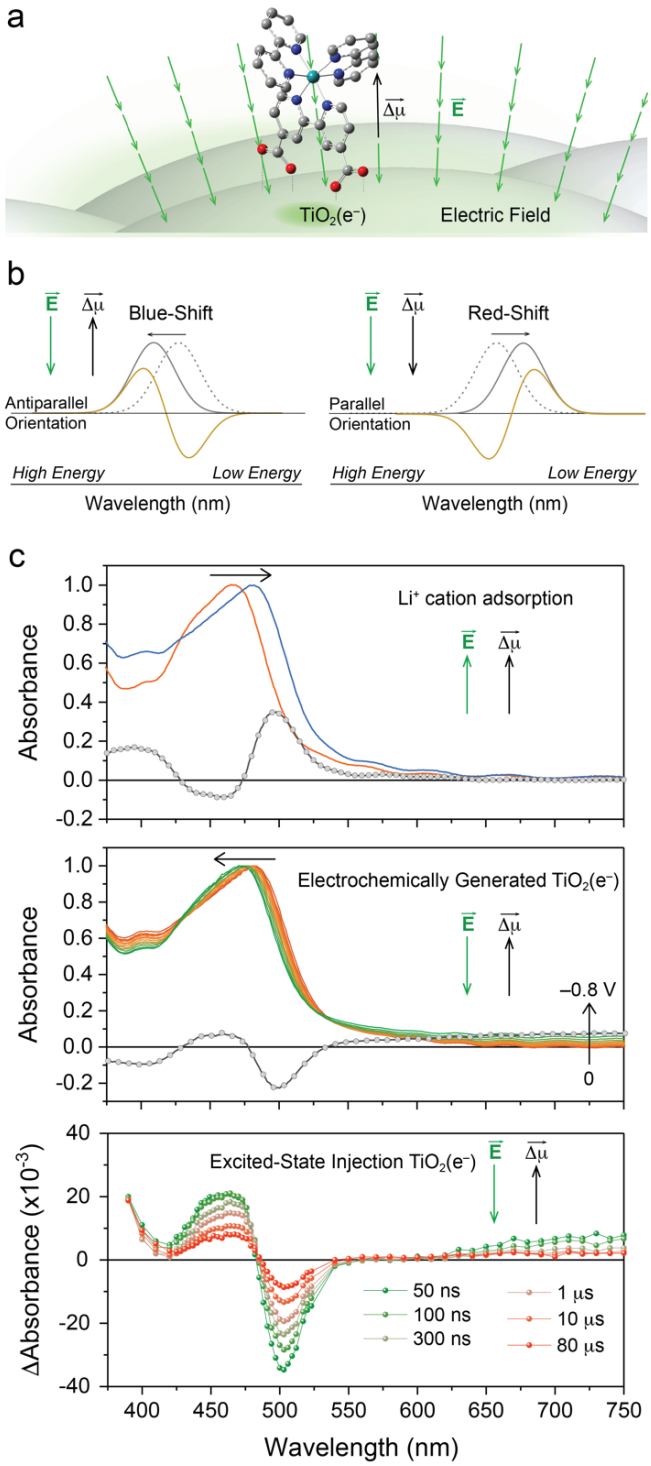

Figure 8. a) An idealized picture of TiO_2|RuC showing an antiparallel orientation of the sensitizer dipole moment change, $\Delta\vec{\mu}$, and the electric field, $\vec{E}$, vectors. b) Explanation of how the relative orientation between $\Delta\vec{\mu}$ and $\vec{E}$ impact the measured spectral shift. The solid and dashed curves are the absorption in the presence and absence of the field, which are typically plotted as the difference spectra shown in yellow. c) The absorption spectra of TiO_2|RuC measured in the presence and absence of Li^+ cations (upper), before and after electrochemical reduction of the TiO_2 (middle), and after pulsed laser excitation and regeneration by iodide.

$$\Delta A = -\frac{dA}{d\nu}\frac{\Delta\vec{\mu}\cdot\vec{E}}{\nu} \qquad (7)$$

The magnitude of $\vec{E}$ has been estimated to be about 2.7 MV cm^{-1} under one sun illumination conditions.[90] This corresponds to a ~40 mV potential drop across the sensitizer. Note that accurate determination of the field strength requires knowledge of $\Delta\vec{\mu}$ that has generally been determined by DFT calculations or extracted from Stark spectra of related sensitizers without the surface binding groups. This uncertainty inspired construction of a traditional Stark apparatus that has shown $\Delta\vec{\mu}$ to be sensitive to functional groups and to spin changes that accompany light absorption.[93,94] Molecular sensitizers with well-defined $\Delta\vec{\mu}$ values positioned precisely at the TiO_2 electrolyte interface can serve as in situ probes of the electric fields present in regenerative and photoelectrosynthetic cells.

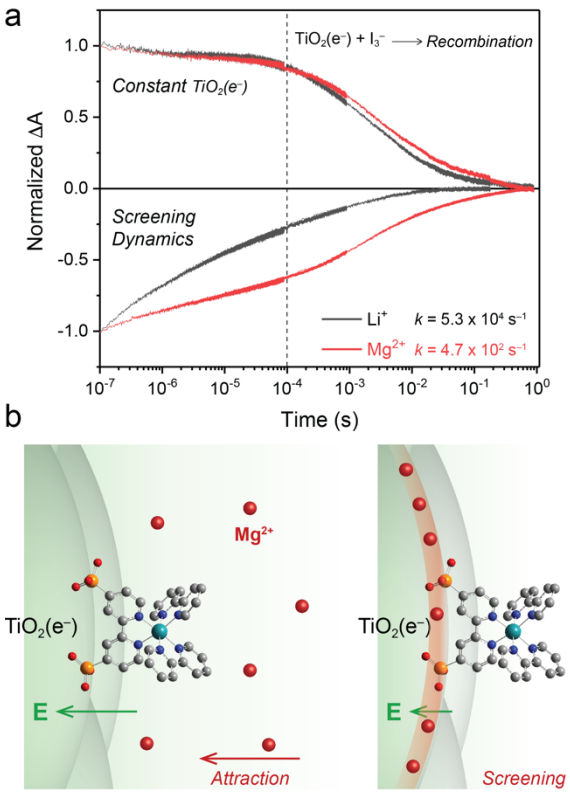

Figure 9. a) Absorption versus log time measured after pulsed 532 nm light excitation of TiO_2|RuC in 0.1 M $LiClO_4$ (black) or $Mg(ClO_4)_2$ (red) and 0.25 M TBAI. The positive absorption tracks the $[I_3^-]$ and $TiO_2(e^-)$ concentrations while the bleach monitors the electro-absorption feature associated with the electric field. Note that at times less than 100 μs (dashed line) the field is constant yet the electro-absorption feature decays with cation dependent kinetics fit to the KWW function, behavior attributed to charge screening. b) Idealized model for the screening response of Mg^{2+} cations (orange spheres) to the electric field created by excited-state injection.

i. Screening Dynamics. The electro-absorption amplitude associated with $\vec{E}$ is known to decrease over time periods where the $TiO_2(e^-)$ concentration is constant. This behavior is attributed

to screening of the field experienced by the sensitizer through ion migration. Kinetic data for charge screening before the dashed 100 μs line in **Figure 9a** are well described by KWW model. The 5.3 x 10^4 s^{-1} rate constant measured in the Li^+ electrolyte indicated an ability to more rapidly screen the field than a Mg^{2+} containing electrolyte, 4.7 x 10^2 s^{-1}.[99] The first-derivative shape is maintained through the screening process implying that the cations insert themselves between the sensitizer and TiO_2, **Figure 9b**.

Electron transfer from TiO_2 to triiodide is most rapid with the Li^+ electrolyte cations, implying that more effective screening results in faster recombination with anionic I_3^-.[100] Study with a series of Lewis acidic cations support this implication and provided rate constants that increased in the order $Na^+ > Li^+ > Mg^{2+} > Ca^{2+}$.[97] However, this same cation trend was found with neutral donors, such as triphenylamines and phenothiazine, that are mono-cations after electron transfer which precludes such a simple interpretation.[98] Although electric fields are well known to impact ions and polar molecules,[100-105] these Coulombic interactions are not, as was previously thought,[100] the predominant factor controlling recombination. Free energy considerations, the diffusion length of the injected electron, and reaction sphere models described in more detail below are now thought responsible for the cation dependent reduction of I_3^-. This reaction is kinetically sluggish, providing a large time window to monitor screening, as the one electron reduction of I_3^- is thermodynamically uphill.[40]

ii. First-Order Recombination to Electrostatically Bound Acceptors. Detailed mechanistic studies of charge recombination have failed to reveal the origin(s) of the irradiance dependent, non-exponential kinetics for charge recombination.[34] An interesting breakthrough came when conditions were identified where recombination displayed first-order kinetics.[89,106] In these studies, dye-sensitization was utilized to quantify the reaction of TiO_2 electrons with oxidized triphenylamines $TiO_2(e^-) + TPA^+ \rightarrow TiO_2 + TPA$. The triphenyl amines were linked to the sensitizer, the TiO_2 surface, or were dissolved in an external 0.1 M $LiClO_4/CH_3CN$ electrolyte, **Figure 10**. The activation energies were small for the solution phase TPAs, 12.5 kJ/mol, relative to that anchored to the TiO_2 surface (23 kJ/mol) or covalently linked to the sensitizer (27 kJ/mol). As a reference point, activation energies to a family of three Ru trisbipyridyl sensitizers (measured in the absence of TPA) was on average 20 $\pm$ 3 kJ/mol.[89,106]

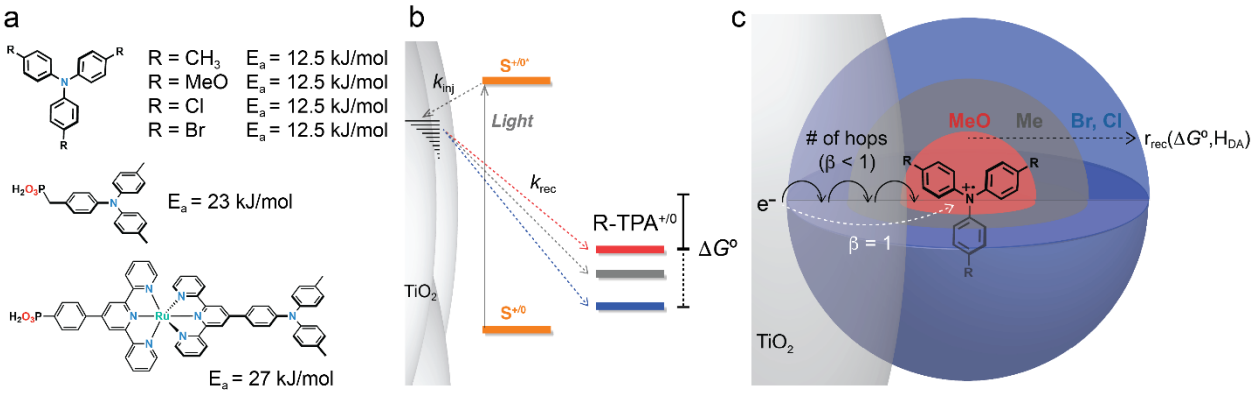

Figure 10. a) The TPA compounds utilized and the measured activation barriers for the recombination reactions. b) The dye-sensitization mechanism utilized to generate the $TiO_2(e^-)$ and TPA^+ reactants. c) Reaction sphere model for the TPA in fluid solution. When the driving force for electron transfer was large (red) electron transfer followed a first-order kinetic model consistent with transfer from TiO_2 directly to the MeO-TPA^+, while increasingly dispersive kinetics were observed as $-\Delta G^o$ decreased from black to blue.

The four solution TPAs had tuned formal $E^o(TPA^{+/0})$ reduction potentials that spanned a 0.5 eV range. First-order kinetics were only measured when the thermodynamic driving force for electron transfer was large.[106] This represented a non-intuitive finding as one would reasonably anticipate a second-order recombination reaction, $r = k[TPA^+][TiO_2(e^-)]$.[55] Note however that under these conditions the TPA^+ acceptor does not undergo lateral hole hopping, as an oxidized sensitizer would, and the $TiO_2(e^-)$ was stabilized by a $LiClO_4$ acetonitrile electrolyte.

The first-order reactivity indicated that strong Coulombic forces held the TPA^+ near the surface such that recombination occurred in a unimolecular type step. When the driving force was less favorable, dispersive KWW kinetics were observed. An Onsager-Perrin-like reaction sphere model was proposed where the tunneling distance was proportional to the free energy change, **Figure 10c**. Activation energies were the same within experimental error 12.5 kJ mol^{-1} for the solution phase TPA^+ acceptors, indicating that the barriers for electron transport and interfacial transfer were similar. The average rate constants increased with $-\Delta G^o$, consistent with electron transfer in the Marcus normal region. The data imply that when the electronic coupling to remote acceptors is small, first-order recombination is possible.[89,106] This finding is supported by more recent studies on conductive oxides described in Section D*iv*.

iii. Sensitizer Flipping. The time dependence of electric fields present after pulsed light excitation is inherently difficult to quantify as it requires deconvolution of relatively small spectral shifts in the presence of large absorption changes associated with the oxidized sensitizers. It is for this reason that the electro-absorption feature went undiscovered in the dye-sensitized field for so long.[90,91] The sensitizer $[Ru(NH_3)_5(ina)]^{2+}$ with $\Delta\vec{\mu} = 9.1$ D, was found to be a sensitive *in situ* probe for time dependent electric field determinations.[106] Pulsed laser excitation of

$TiO_2|Ru(NH_3)_5$(ina) in neat CH_3CN led to a time dependent blue shift of the absorption bleach, **Figure 11a**. The transient spectra were quantitatively modeled by a sum of contributions from the electric field and the $TiO_2(e^-)|Ru^{III}(NH_3)_5$(ina) charge separated state, **Figure 11b**. The average rate constant for electric field contraction was within experimental error the same as that for charge recombination, $k = 6.8 \times 10^4\ s^{-1}$ **Figure 11c**. This suggested the presence of a homogeneous field strength that contracted as recombination and the number of injected electrons decreased. In the presence of Li^+ electrolyte cations $\vec{E}$ contracted about ten-times faster, behavior consistent with an increased interfacial permittivity and charge screening.

Light excitation of the ethyl ester derivative $TiO_2|Ru(NH_3)_5$(eina), resulted in spectroscopic changes quite distinct from the carboxylic acid analogue, **Figure 11**. The absorption spectra displayed an initial bleach that evolved with time into a first-derivative spectra whose sign indicated that the sensitizers had flipped over.[108] Importantly, the spectral signature of the flipped sensitizers persisted after charge recombination was complete and the field associated with the injected electrons was gone. This indicated that the flipped molecules were metastable on the oxide surface. Decay-associated spectra, DAS, allowed extraction of the rate constants for charge recombination and for flipping, **Figures 11e** and **11f**. Kinetic isotope studies with $TiO_2|Ru(ND_3)_5$(eina), revealed $k_H/k_D = 26.7$ and 0.12 for charge recombination and for flipping, respectively. In all cases, charge recombination was more rapid when the oxidized sensitizer was flipped over, behavior attributed to strong electronic coupling through the amine hydrogen atoms.[109]

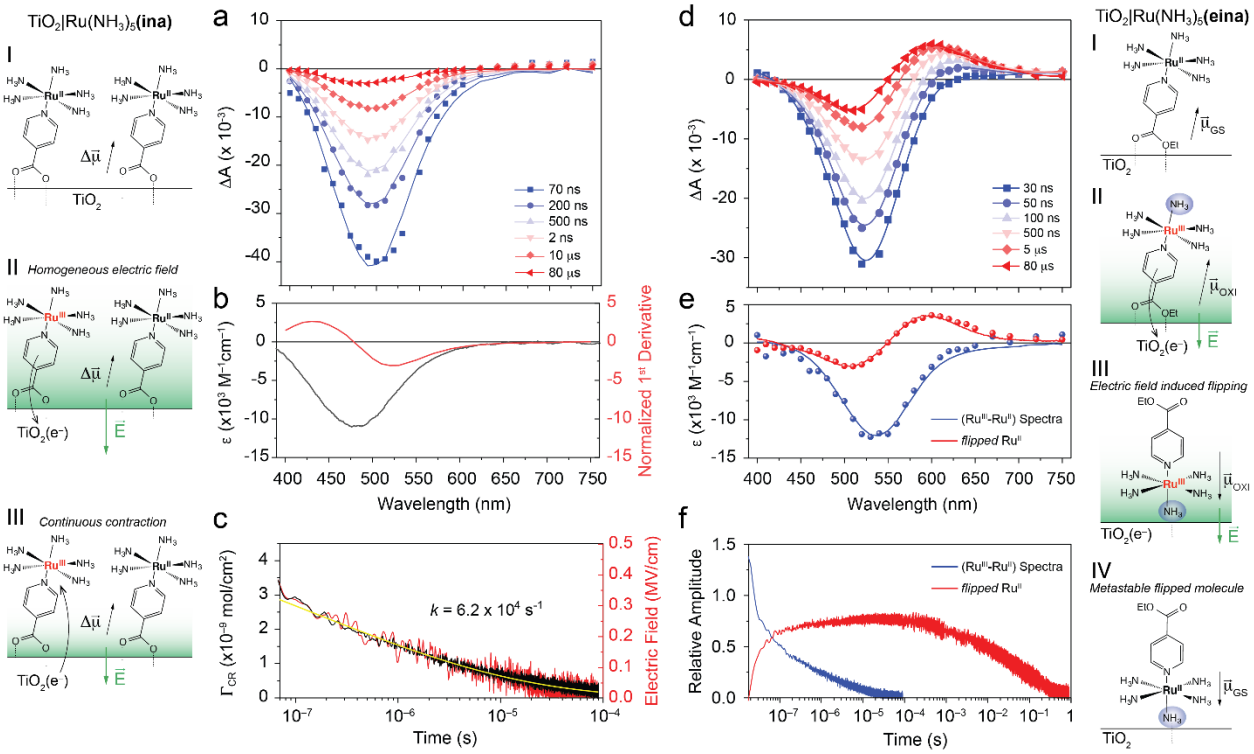

Figure 11. a) Absorption difference spectra measured after pulsed light excitation of TiO_2|$Ru(NH_3)_5$(ina) with overlaid spectral simulations based on linear combinations of the spectra shown in b). b) Absorption difference spectrum for Ru^{III}–Ru^{II} and the 1st derivative of the TiO_2|$Ru(NH_3)_5$(ina) ground-state spectrum used to quantify the magnitude of the surface electric fields. c) Representative kinetic data for charge combination and electric field strength. d) Absorption difference spectra measured after pulsed light excitation of TiO_2TiO_2|$Ru(NH_3)_5$(eina) with overlaid spectral simulations based on linear combinations of the spectra shown in e). e) Decay-associated spectra obtained from kinetic analysis of the transient data. f) Kinetic data for charge recombination and molecular flipping.

The electric field induced by excited state injection created a torque sufficient to flip these weakly anchored sensitizers.[108] Flipping was absent with the more strongly binding carboxylic acid ina derivative and with SnO_2/TiO_2 core/shell materials that presumably screen the field experienced by the sensitizers more effectively. Spectro-electrochemical data showed that a 10-fold larger field strength was required to flip the sensitizers in the Ru(II) formal oxidation state, indicating that the increased acidity of the amines in the Ru(III) state plays an important role in the light driven creation of the metastable flipped orientation.[110] Overall, the data show that electric fields created at illuminated semiconductor interfaces are sufficient to re-orientate molecules anchored to its surface. In future research, one can imagine utilizing a variety of surface anchoring groups whose flipping behavior reports directly on the underlying electric field strength.[111-115]

iv. Probing the Electric Double Layer. Transparent conductive oxide materials (TCOs) have many practical applications,[116] yet have received relatively little attention for dye-sensitization, in part because it is difficult to generate a significant photovoltage and hence power conversion efficiency in regenerative solar cells. The free electron concentration in a TCO is not appreciably

influenced by excited-state injection. Nevertheless, TCOs support long-lived charge separation when excited-state electron transfer occurs remote to the surface with free energy gradients that direct the electron toward, and the oxidizing equivalent away, from the conductor.[117-119] A layer-by-layer assembly technique with Zr^{IV} Lewis acids was utilized to spatially arrange redox active molecular components on mesoporous thin films of In_2O_3:Sn (nITO) nanocrystallites.[120-123] For the full molecular assembly shown with at terminal triphenyl amine (TPA), long-lived charge separation was achieved with a quantum yield of 0.2 and first-order recombination kinetics (k = 1.5 s^{-1}) to TPA^+, **Figure 12a** and **b**.[118] This data supports the notion that first-order recombination may be more commonly observed with weakly coupled acceptors located outside of the electric double layer.[89,106] Comparative studies revealed that the viologen acceptor and the iron donor were required for such long-lived charge separation. For example, when the TPA was absent, recombination to the Fe^{III} center was about one thousand times faster. Interestingly, there was little kinetic advantage to having the Fe^{II} donor relative to the sensitizer alone. An advantage of the layer-by-layer assembly is hence that the impact of an individual redox active component can be determined without significant synthesis.

When the terminal TPA was replaced by a Ru(bda)-type water oxidation catalyst, long-lived charge separation (k = 0.17 s^{-1}) was again achieved, **Figure 12c**.[124] Activation of water oxidation catalysts to higher oxidation states by proton-coupled electron transfer is difficult as it occurs in competition with charge recombination, yet was clearly observed in these assemblies. Sustained water oxidation was also evident with Faradaic yields that approach 70%. The integration of molecular components onto mesoporous TCO thin films that support long-lived charge separation and water photo-oxidation represent successful demonstrations that conducting materials are viable for applications in solar fuel production.

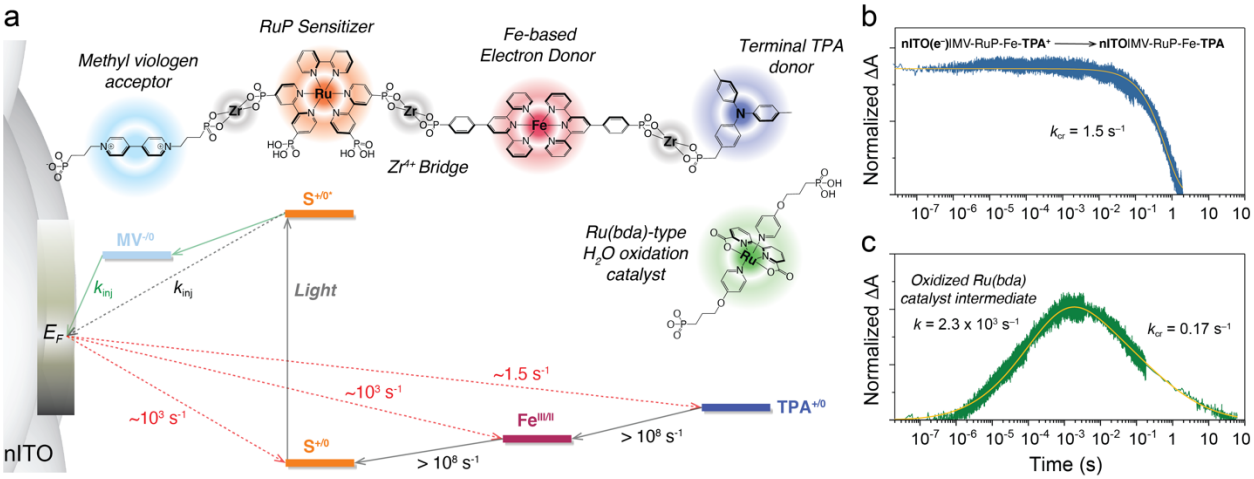

Figure 12. a) Layer-by-layer arrangement of redox active molecular components on In_2O_3:Sn, nITO, with the relative free energy changes and the measured average recombination rate constants. b) The absorption due to TPA^+ plotted vs log time after pulsed 532 nm excitation of the assembly in a). Overlaid on the data is a fit to a first-order kinetic

model. c) Absorption changes due to the oxidized Ru(bda) catalysts shown in a) with overlaid fits to a sum of two KWW functions.

For fundamental electron transfer, the TCO materials may serve as electron acceptors (n-type behavior) or as electron donors (p-type).[125] The Fermi-level of the TCO is of relevance rather than E_{CB} and/or trap states in semiconducting materials. Hence a significant advantage of TCOs is that their metallic character allows potentiostatic control of the Fermi level (E_F) and thus the driving force for electron transfer, $-\Delta G° = nF(E°' - E_F)$.[126,127] By mapping kinetics through Gerischer's distribution, electron transfer to acceptors positioned within the electric double layer, EDL, have been quantified spectroscopically after excited state injection into the TCO.[128,129] This approach holds some similarity to previous electrochemical studies of redox terminated self-assembled monolayers on gold electrodes,[130-134] yet holds promise to be more general and useful, particularly for ultrafast interfacial electron transfer reactivity.

In the classic EDL structure the surface anchoring O and P atoms reside in the inner-Helmholtz plane (IHP) and the redox active site is located in the outer Helmholtz plane, (OHP).[135-138] By systematically positioning redox active groups away from an nITO interface, the diffuse layer was systematically probed in the layer-by-layer approach, **Figure 13a**.[128,129] The redox active TPA and RuP were selected as they have small inner-sphere reorganization energies such that $\lambda = \lambda_i + \lambda_o \sim \lambda_o$.[139-141] Their electrochemical and spectroscopic properties were insensitive to their physical location within the EDL in 0.1 M $LiClO_4/CH_3CN$ electrolyte. In contrast, the free energy dependence of the interfacial electron transfer kinetics were highly sensitive to their location. Light absorption initiates excited state injection and the recombination rate constants were quantified spectroscopically as a function of $-\Delta G°$. **Figure 13b** shows kinetic data for nITO|-$(MeP_2)_n$-TPA with n = 0, 1. The kinetic data were non-exponential, and k_{cr} was approximated as the inverse of the time required for the initial amplitude to decay by half. Marcus-Gerischer analysis allowed determination of λ, **equation 8**,

$$\frac{k_{cr}}{k_{cr}^{max}} = \frac{1}{2}\left[1 - erf\left(\frac{\Delta G° + \lambda}{2\sqrt{\lambda k_B T}}\right)\right] \qquad (8)$$

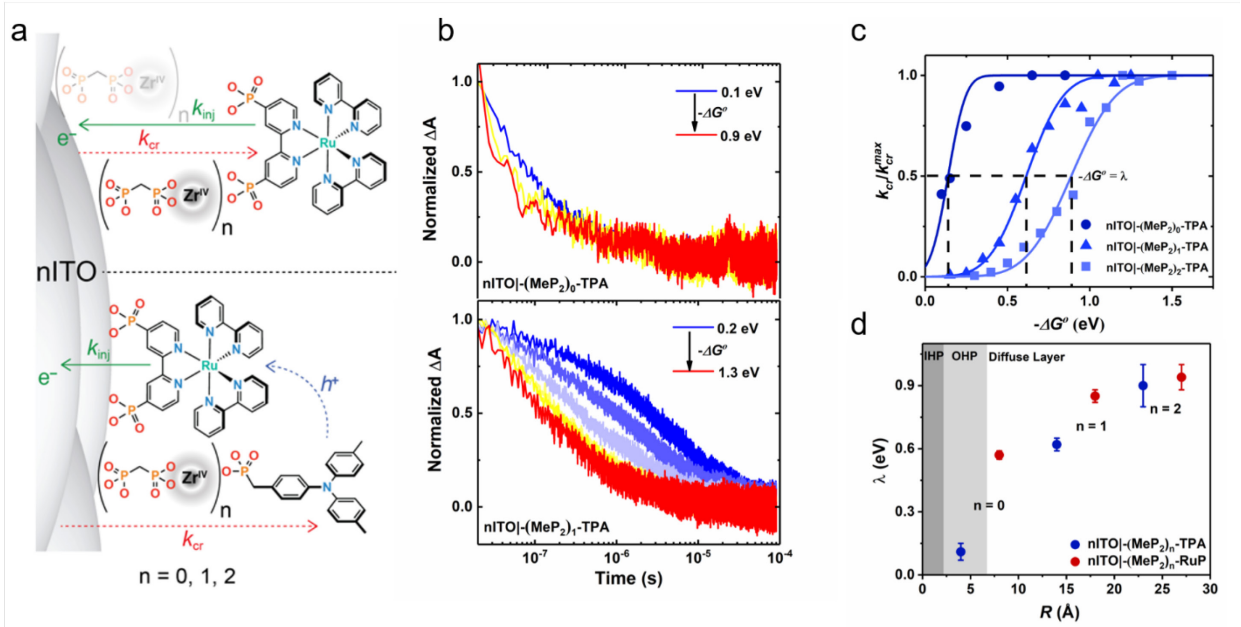

Figure 13. a) Schematic of the approach for initiating electron transfer from nITO to molecular acceptors spaced at different locations within the electric double layer for nITO|-$(MeP_2)_n$-RuP (top) and nITO|-$(MeP_2)_n$-TPA (bottom). Excited-state injection, k_{inj} is initiated with a pulsed laser and the subsequent electron transfer from nITO to TPA^+ or $Ru^{III}P$ (k_{cr}) is quantified spectroscopically as a function of the applied potential. b) Charge recombination kinetic data for the indicated assemblies as a function of $-\Delta G°$. c) Plot of $\frac{k_{cr}}{k_{cr}^{max}}$ versus $-\Delta G^o$ with overlaid fits to the Marcus-Gerischer expression in equation 8. d) The λ values *vs* distance R for nITO|-$(MeP_2)_n$-RuP (red circles) and nITO|-$(MeP_2)_n$-TPA (blue circles) for data obtained with a 0.1 M $LiClO_4/CH_3CN$ electrolyte.

Gerischer's prediction of activationless electron transfer when $-\Delta G° > 2\lambda$, where the maximum rate constant, k_{cr}^{max}, is independent of the driving force was evident in this data, **Figure 13c**. The $-\Delta G°$ value at ½ k_{cr}^{max} is equal to λ and values so quantified as a function of distance revealed a remarkable result: λ is near zero when the redox active group is present within the OHP, **Figure 13d**. Very similar data were obtained with aqueous electrolytes.[129] As the outer-sphere reorganization is expected to control the barrier for electron transfer, the data indicates fast and barrierless transfer within the Helmholtz planes. At distances greater than ~20 Å in the diffuse layer, λ approximately equals the value expected for homogeneous reactions, $\lambda \approx 0.9$ eV. Such data could not be modelled by dielectric continuum models and required higher levels of theory that take into account the greatly reduced dielectric constant within the Helmholtz planes.[142-144] This dye-sensitization approach provides exciting opportunities to test interfacial electron transfer theories and to probe the impact of the electric double layer on electron transfer and catalysis.

As one final example of the utility of conductive oxides for fundamental mechanistic study, the reorganization energy for proton-coupled electron transfer, λ_{PCET},[145] of the water oxidation catalyst $[Ru^{II}(tpy)(4,4'\text{-}(PO_3H_2)_2\text{-}bpy)OH_2]^{2+}$ (Ru^{II}-OH_2) was quantified.[146,147] Pourbaix diagrams indicate that for pH > 2, oxidation results in the loss of an electron from the metal and a proton from the coordinated water molecule. For this reason, the recombination reaction between nITO

and the oxidized catalyst was tuned above and below the pKa of Ru^{III}-OH_2 to occur with ($2 \leq pH \leq 5$) and without ($pH < 1.7$) proton involvement. The kinetic data revealed that the reduction from Ru^{III}-OH to Ru^{II}-OH_2 required 0.4 eV higher reorganization energy than did the pure electron transfer reaction. Future studies in which the PCET acceptor is positioned with the EDL are expected to provide insights into how the oxide interface influences λ_{PCET} that is of direct relevance to water oxidation.[145,148]

Conclusions and Future Perspectives

The mesoporous nanocrystalline TiO_2 thin films introduced in 1991 have provided outstanding opportunities for fundamental molecular-level characterization of interfacial electron transfer. These materials offer combined high surface area and visible transmittance for spectroscopic analysis with high stability in electrolyte solutions for photo- and electrochemical measurements. The electron transfer kinetics are often understood through Gerischer diagrams yet in some cases, like charge recombination, the observed rate constants are also impacted by hole-hopping and/or transport of the injected electrons. The discovery of an electro-absorption feature provides direct information on the magnitude of the electric field, the sensitizer orientation, and charge-screening dynamics that are not easily elucidated by other means. Regeneration through iodide oxidation studies implicate inner-sphere electron transfer pathways with some sensitizers. Acceptor-bridge-donor sensitizers provide a means to photo-initiate redox equilibria providing keen insights into the impact of electronic coupling on intramolecular electron transfer.

With these advances it is worthwhile to consider the *future* of dye-sensitized semiconductors from the viewpoint of the two most commonly envisioned applications: Regenerative and Photoelectrosynthetic Cells. Below these applications and discussed with reference to the fundamental studies described in the previous section (**A-D**) and the relevant literature.

Regenerative Solar Cells. The confirmed 12.3% efficiency of dye-sensitized solar cells under air-mass 1.5 conditions is not yet competitive with emerging perovskite solar cells or with conventional photovoltaics,[149] but they continue to be pursued for low light and window applications where they often outperform traditional Si photovoltaics.[150-152] Our ability to quantify electric fields and ion migration dynamics as a function of solar irradiance will likely allow under further optimization for these conditions (**D.i-iii**). A significant energy loss is associated with the iodide/tri-iodide redox mediator that include non-quantitative regeneration at the power point condition (decreasing fill-factors) and significant free energy losses associated with a disproportionation reaction (decreasing open circuit photovoltages). The 'inner-sphere' strategies (**B.i-ii**) enhance regeneration while the A-B-D sensitizers (**C.iii**) buy more time for iodide oxidation by slowing recombination. However, alternative redox mediators seems necessary for >

5% efficiency increases. Promising $Co^{III/II}$ [153-155] and $Cu^{II/I}$ [156-160] mediators continue to be pursued that possess significant structural changes with electron transfer that may inspire discovery of new classes of mediators.[161,162] An additional benefit of the $Cu^{II/I}$ mediators is that they function in the absence of an external solvent[160] and these as well as solid-state hole transport materials[163] continue to offer the promise of greatly enhanced performance. A novel idea is to use lateral hole-hopping as a means to collect the oxidizing equivalents at the counter-electrode,[164] however the efficiencies obtained by this approach have thus far been very low. The identification of new redox mediators that enable large open circuit photovoltages, sensitizers with increased absorption in the near infrared, and solid state hole-conductors represent key next steps for practical applications as regenerative solar cells.

Photoelectrosynthesis Cells. Water splitting continues to be the target of dye-sensitized photoelectrosynthesis cells.[5] The general idea is to sensitize the TiO_2 in the celebrated Fujishima-Honda cell to visible light with molecular dyes.[165] However, unlike iodide oxidation, water oxidation to O_2 requires four oxidizing equivalents and is both kinetically and thermodynamically more demanding. One strategy is to utilize redox mediators to deliver oxidizing equivalents to a catalyst of a tandem photoelectrode positioned away from the dye-sensitized semiconductor interface.[166,167] A more common strategy is to integrate water oxidation catalysts into the dye-sensitized oxide interface (**D.iv**).[5,168-170] However, water oxidation is slow relative to recombination even with the most well optimized catalysts.[171] Therefore, materials or sensitizers that inhibit recombination (**C.iii**) and catalysts with higher turnover frequencies are critically needed. Note that the turnover frequencies of most water oxidation catalysts increase with pH, while the excited state injection yields and durability decrease in alkaline solutions (**A.iii**). The creation of carefully designed architectures that enable quantitative injection at the dye-sensitized interface with hole-transfer to weakly coupled water oxidation catalysts present in an alkaline environment would be impactful. The creation of such a highly organized interface that is also thermodynamically stable remains a challenging and important goal.

An intriguing idea is to utilize the electrons injected into TiO_2 for proton or CO_2 reduction. This idea is particularly appealing as p-type oxide materials that could serve in a similar manner are severely lacking. The injected electrons are well formulated as localized Ti^{III} states whose reducing power can be widely tuned with electrolyte cations (**A.ii-iii**) and with solvent.[172,173] They are potent one-electron reductants, but do not efficiently drive the multi-electron transfer reactions necessary for solar fuel generation. Studies with radical clocks have provided a time scale for sequential one-electron transfer reactivity.[174,175] With surface anchored catalysts there is also evidence that inner-sphere two-electron transfer pathways can be accessed.[176] Colloidal TiO_2 and related metal oxide nanoparticles have been shown to participate in proton-coupled electron

transfer (PCET) reactions (**D.iv**) with organic reactants.[177-180] Taken together this prior work indicates that multi-electron and PCET reactivity with catalysts positioned at precise locations within the electric double layer provide the possibility to drive reduction reactions that produce solar fuels from water and CO_2 far more efficiently.

Photoelectrosynthesis cells that would yield high value organic compounds for applications in medicine and biotechnology embody an emerging area for dye-sensitization. So-called 'photoredox chemistry' is typically performed in fluid solution with sacrificial reagents, sensitizers (often called photocatalysts in this field) and organic reactants.[181-183] An alternative approach is to photoinitiate the organic transformations within the pores of dye-sensitized mesoporous thin films.[184] With transparent conductive oxides (**D.iv**), reducing and/or oxidizing equivalents can be photogenerated for oxidative or reductive catalysis. This approach minimizes reaction volumes, facilitates isolation of the desired products, and enables more facile reuse of the molecular photocatalysts/sensitizers. In principle, sacrificial reagents could be eliminated completely with improved efficiency on an absorbed photon basis. Indeed, the quantitative ultrafast excited state injection (**A.i**) removes the present restriction of sufficiently long-lived excited state that are necessary for diffusional quenching by sacrificial reagents. By increasing efficiency, detailed insights into the mechanisms of the organic transformations enabled by these high surface area materials can be elucidated by the techniques described throughout this Perspective. Indeed, the use of mesoporous thin films in photoelectrosynthesis cells to produce high-value organic compounds represent a promising direction for future research for dye-sensitized mesoporous thin films.

Acknowledgments

The water oxidation and studies of sensitized conductive oxides conducted by J.S. and L.T.-G were supported as part of the Alliance for Molecular PhotoElectrode Design for Solar Fuels (AMPED), an Energy Frontier Research Center (EFRC) funded by the U.S. Department of Energy, Office of Science, Office of Basic Energy Sciences under Award Number DE-SC0001011. L.T.-G. is now a Postdoctoral researcher of the Fonds de la Recherche Scientifique – FNRS. The lateral hole-hopping studies by K.H. were funded by the National Science Foundation under Award CHE-1465060. The electric field and Stark spectroscopic studies of R.S. were funded by Division of Chemical Sciences, Office of Basic Energy Sciences, Office of Energy Research, US Department of Energy (Grant DE-SC0013461).

Author Information

Corresponding Author:
*E-mail: gjmeyer@email.unc.du

Notes: The author declare no competing financial interest.

References

1. Neblette, C.B., Fundamentals of Photography, Van Norstrand Reinhold Co., Princeton, N.J., 1970.
2. Gerischer, H.; Tributsch, H., Elektrochemische Untersuchungen zur spektralen Sensibilisierung von ZnO-Einkristallen. *Berich. Bunsen. Gesell.* **1968,** *72* (3), 437-445.
3. Tributsch, H.; Gerischer, H., The use of semiconductor electrodes in the study of photochemical reactions. *Berich. Bunsen. Gesell.* **1969,** *73*, 850-854.
4. Tributsch, H.; Gerischer, H., Elektrochemische Untersuchungen über den Mechanismus der Sensibilisierung und übersensibilisierung an ZnO-Einkristallen. *Berich. Bunsen. Gesell.* **1969,** *73* (3), 251-260.
5. Youngblood, W.J.; Lee, S-H.A.; Maeda, K.; Mallouk, T.E. Visible Light Water Splitting Using Dye-Sensitized Oxide Semiconductors. *Acc. Chem. Res.* **2009**, *42*, 1966-1973.
6. O'Regan, B.; Grätzel, M., A low-cost, high-efficiency solar cell based on dye-sensitized colloidal TiO_2 films. *Nature* **1991,** *353*, 737-740.
7. Grätzel, M. Dye-sensitized solar cell. *J. Photochem. Photobiol. C: Photochem. Rev.* **2003**, *4*, 145-153.
8. Hagfeldt, A.; Boschloo, G.; Sun, L.; Kloo, L.; Pettersson, H. Dye Sensitized Solar Cells. *Chem. Rev.* **2010**, *110*, 6595-6663.
9. Campagna, S.; Puntoriero, F.; Nastasi, F.; Bergamini, G.; Balzani, V. Photochemistry and photophysics of coordination compounds: ruthenium. *Top. Curr. Chem.* **2007,** *280*, 117–214.
. Zigler, D. F.; Morseth, Z. A.; Wang, L.; Ashford, D. L.; Brennaman, M. K.; Grumstrup, E. M.; Brigham, E. C.; Gish, M. K.; Dillon, R. J.; Alibabaei, L.; Meyer, G. J.; Meyer, T. J.; Papanikolas, J. M., Disentangling the Physical Processes Responsible for the Kinetic Complexity in Interfacial Electron Transfer of Excited Ru(II) Polypyridyl Dyes on TiO_2. *J. Am. Chem. Soc.* **2016,** *138*, 4426-4438.
11. Tachibana, Y.; Haque, S. A.; Mercer, I. P.; Moser, J. E.; Klug, D. R.; Durrant, J. R., Modulation of the Rate of Electron Injection in Dye-Sensitized Nanocrystalline TiO_2 Films by Externally Applied Bias. *J. Phys. Chem. B* **2001,** *105*, 7424-7431.
12. Asbury, J. B.; Hao, E.; Wang, Y.; Ghosh, H. N.; Lian, T., Ultrafast Electron Transfer Dynamics from Molecular Adsorbates to Semiconductor Nanocrystalline Thin Films. *J. Phys. Chem. B* **2001,** *105*, 4545-4557.
13. Gundlach, L.; Willig, F. Ultrafast Photoinduced Eletron Transfer at Electrodes: The General Case of Heterogeneous Electron-Transfer Reaction. *ChemPhysChem.* **2012***, 12,* 2877-2881.
14. McCusker, J. K. Femtosecond Absorption Spectroscopy of Transition Metal Charge-Transfer Complexes. *Acc. Chem. Res.* **2003**, *36*, 876–887.
15. Carey, M. C.; Adelman, S. L.; McCusker, J. K. Insights into the Excited State Dynamics of Fe(II) Polypyridyl Complexes from Variable-Temperature Ultrafast Spectroscopy. *Chem. Sci.* **2019**, *10*, 134–144.
16. Auböck, G.; Chergui, M. Sub-50-Fs Photoinduced Spin Crossover in $[Fe(bpy)_3]^{2+}$ *Nat. Chem.* **2015**, *7*, 629–633.

17. Xia, H.-L.; Ardo, S.; Narducci Sarjeant, A. A.; Huang, S.; Meyer, G. J. Photodriven Spin Change of Fe(II) Benzimidazole Compounds Anchored to Nanocrystalline TiO_2 Thin Films. *Langmuir* **2009,** *25*, 13641-13652.
18. Fredin, L. A.; Pápai, M.; Rozsályi, E.; Vankó, G.; Wärnmark, K.; Sundström, V.; Persson, P., Exceptional Excited-State Lifetime of an Iron(II)–N-Heterocyclic Carbene Complex Explained. *J. Phys. Chem. Lett.* **2014,** *5*, 2066-2071.
19. Harlang, T. C. B.; Liu, Y.; Gordivska, O.; Fredin, L. A.; Ponseca, C. S.; Huang, P.; Chábera, P.; Kjaer, K. S.; Mateos, H.; Uhlig, J.; Lomoth, R.; Wallenberg, R.; Styring, S.; Persson, P.; Sundström, V.; Wärnmark, K. Iron sensitizer converts light to electrons with 92% yield. *Nature Chem.* **2015,** *7*, 883-889.
20. Liu, Y.; Persson, P.; Sundström, V.; Wärnmark, K. Fe N-Heterocyclic Carbene Complexes as Promising Photosensitizers. *Acc. Chem. Res.* **2016**, *49*, 1477–1485.
21. Chábera, P.; Kjaer, K.S.; Prakash, O.; Honarfar, A,; Liu, Y.; Fredin, L.A.; Harlang, T.C.B.; Lidin, S.; Uhlig, J.; Sundström, V.; Lomoth, R.; Persson, P.; Wärnmark, K. Fe^{II} Hexa N-Heterocyclic Carbene Complex with a 528 ps Metal-to-Ligand Charge-Transfer Excited-State Lifetime. *J. Phys. Chem. Lett.* **2018,** *9*, 459-463.
22. Zimmer, P.; Burkhardt, L.; Friedrich, A.; Steube, J.; Neuba, A.; Schepper, R.; Müller, P.; Flörke, U.; Huber, M.; Lochbrunner, S.; Bauer, M. The Connection between NHC Ligand Count and Photophysical Properties in Fe(II) Photosensitizers: An Experimental Study. *Inorg. Chem.* **2018,** *57*, 360-373.
23. Brigham, E.; Achey, D.; Meyer, G.J. Excited State Electron Transfer from Cobalt Coordination Compounds Anchored to TiO_2. *Polyhedron* **2014**, *82*, 181-190.
24. Vrachnou, E.; Vlachopoulos, N.; Grätzel, M. Efficient visible light sensitization of TiO_2 by surface complexation with $Fe(CN)_6^{4-}$. *J. Chem. Soc. Chem. Comm.* **1987,** *12*, 868-870.
25. Yang, M.; Thompson, D. W.; Meyer, G.J. Charge-Transfer Studies of Iron Cyano Compounds Bound to Nanocrystalline TiO_2 Surfaces. *Inorg. Chem.* **2002,** *41*, 1254-1262.
26. Creutz, C.; Brunschwig, B.S.; Sutin, N. Interfacial Charge-Transfer Absorption: 3. Application to Semiconductor−Molecule Assemblies. *J. Phys. Chem. B* **2006,** *110*, 25181-25190.
27. Harris, J.A.; Trotter, K.; Brunschwig, B.S. Interfacial Electron Transfer in Metal Cyanide-Sensitzied TiO_2 Nanoparticles. *J. Phys. Chem. B* **2007**, *111*, 6695-6702.
28. De Angelis, F.; Tilocca, A.; Selloni, A. Time-Dependent DFT Study of $[Fe(CN)_6]^{4-}$ Sensityization of TiO_2 Nanoparticles. *J. Am. Chem. Soc.* **2004,** *126*, 415024-15025.
29. Finklea, H. O. *Semiconductor electrodes*. Elsevier: Amsterdam, The Netherlands, 1988.
30. Connor, P.A.; Dobson, K.D.; McQuillan, A.J. Infrared Spectroscopy of the TiO_2/Aqueous Solution Interface. *Langmuir* **1999**, *15*, 2402-2408.
31. Lyon, L. A.; Hupp, J. T. Energetics of the Nanocrystalline Titanium Dioxide/Aqueous Solution Interface: Approximate Conduction Band Edge Variations between $H_0 = -10$ and $H_- = +26$ *J. Phys. Chem.* **1995**, 99, 15718.
32. Clark, W. D. K.; Sutin, N. Spectral sensitization of n-type titanium dioxide electrodes by polypyridineruthenium(II) complexes. *J. Am. Chem. Soc.* **1977,** *99*, 4676-4682.
33. Watson, D. F.; Marton, A.; Stux, A. M.; Meyer, G. J. Influence of Surface Protonation on the Sensitization Efficiency of Porphyrin-Derivatized TiO_2. *J. Phys. Chem. B* **2004**, *108*, 11680-11688.
34. Kelly, C. A.; Farzad, F.; Thompson, D. W.; Stipkala, J. M.; Meyer, G. J. Cation-Controlled Interfacial Charge Injection in Sensitized Nanocrystalline TiO_2. *Langmuir* **1999**, *15*, 7047-7054.

35. Rothenberger, G.; Fitzmaurice, D.; Gratzel, M. Spectroscopy of conduction band electrons in transparent metal oxide semiconductor films: optical determination of the flatband potential of colloidal titanium dioxide films. *J. Phys. Chem* **1992**, *96*, 5983-5986.
36. Boschloo, G.; Fitzmaurice, D. Spectroelectrochemical Investigation of Surface States in Nanostructured TiO_2 Electrodes. *J. Phys. Chem. B* **1999**, *103*, 2228-2231.
37. Boschloo, G.; Fitzmaurice, D. Electron Accumulation in Nanostructured TiO_2 (Anatase) Electrodes. *J. Phys. Chem. B* **1999**, *103*, 7860-7868.
38. Davis, V. K.; Sampaio, R. N.; Marquard, S. L.; Meyer, G. J., Electric Fields Detected on Dye-Sensitized TiO_2 Interfaces: Influence of Electrolyte Composition and Ruthenium Polypyridyl Anchoring Group Type. *J. Phys. Chem. C* **2018**, *122*, 12712-12722.
39. Morris, A.J.; Meyer, G.J. TiO_2 Surface Functionalization to Control the Density of States. *J. Phys. Chem. C* **2008**, *112*, 18224-18231.
40. Wu, J. Lan, Z.; Lin, J.; Huang, M.; Huang, Y.; Fan, Luo, G. Electrolytes in Dye-Sensitized Solar Cells. *Chem. Rev.* **2015**, *115*, 2136-2173.
41. Boschloo, G.; Hagfeldt, A. Characteristics of the Iodide/Triiodide Redox Mediator in Dye-Sensitzed Solar Cells. *Acc. Chem. Res.* **2009**, *42*, 1819-1826.
42. Robson, K.C.D.; Hu, K.; Meyer, G.J.; Berlinguette, C.P. Atomic Level Resolution of Dye Regeneration in the Dye-Sensitized Solar Cell. *J. Am. Chem. Soc.* **2013**, *135*, 1961-1971.
43. Li, F; Jennings, R.J.; Wang, Q. Regeneration Efficiency in Dye-Sensitized Solar Cells. *ACS Nano* **2013**, *7*, 8233-8242.
44. Haque, S. A.; Tachibana, Y.; Willis, R. L.; Moser, J. E.; Grätzel, M.; Klug, D. R.; Durrant, J. R. Parameters Influencing Charge Recombination Kinetics in Dye-Sensitized Nanocrystalline Titanium Dioxide Films. *J. Phys. Chem. B* **2000**, *104*, 538– 547.
45.
46. Simon, S. J. C.; Parlane, F. G. L.; Swords, W. B.; Kellett, C. W.; Du, C.; Lam, B.; Dean, R. K.; Hu, K.; Meyer, G. J.; Berlinguette, C. P. Halogen Bonding Promotes Higher Dye-Sensitized Solar Cell Photovoltages. *J. Am. Chem. Soc.* **2016**, *138*, 10406-10409.
47. Parlane, F. G. L.; Mustoe, C.; Kellett, C. W.; Simon, S. J.; Swords, W. B.; Meyer, G. J.; Kennepohl, P.; Berlinguette, C. P. Spectroscopic detection of halogen bonding resolves dye regeneration in the dye-sensitized solar cell. *Nature Comm.* **2017**, *8*, 1761.
48. Kellett, C. W.; Swords, W. B.; Turlington, M. D.; Meyer, G. J.; Berlinguette, C. P., Resolving orbital pathways for intermolecular electron transfer. *Nature Comm.* **2018**, *9*, 4916.
49. Metrangolo, P.; Neukirch, H.; Pilati, T.; Resnati, G., Halogen Bonding Based Recognition Processes: A World Parallel to Hydrogen Bonding. *Acc. Chem. Res.* **2005**, *38*, 386-395.
50. Cavallo, G.; Metrangolo, P.; Milani, R.; Pilati, T.; Priimagi, A.; Resnati, G.; Terraneo, G. The Halogen Bond *Chem. Rev*. **2016**, *116*, 2478–2601.
51. Erdélyi, M. Halogen bonding in solution. *Chem. Soc. Rev.* **2012**, *4*1, 3547-3557.
52. Taube, H.; Myers, H.; Rich, R. L. Observations on the Mechanism of Electron Transfer in Solution. *J. Am. Chem. Soc.* **1953**, *75*, 4118-4119.
53. Brunschwig, B.S.; Creutz, C.; Sutin, N. Optical transitions of symmetrical mixed-valence systems in the Class II–III regime". *Chem. Soc. Rev.* **2002**, *31*,168–184.
54. Casarin, L.; Swords, W. B.; Caramori, S.; Bignozzi, C. A.; Meyer, G. J. Rapid Static Sensitizer Regeneration Enabled by Ion Pairing. *Inorg. Chem.* **2017**, *56*, 7324-7327.
55. Xu, P.; Gray, C. L.; Xiao, L.; Mallouk, T. E., Charge Recombination with Fractional Reaction Orders in Water-Splitting Dye-Sensitized Photoelectrochemical Cells. *J. Am. Chem. Soc.* **2018**, *140,* 11647-11654

56. Nazeeruddin, M. K.; Kay, A.; Rodicio, I.; Humphry-Baker, R.; Mueller, E.; Liska, P.; Vlachopoulos, N.; Graetzel, M. Conversion of light to electricity by cis-X_2 bis(2,2'-bipyridyl-4,4'-dicarboxylate)ruthenium(II) charge-transfer sensitizers (X = Cl^-, Br^-, I^-, CN^-, and SCN^-) on nanocrystalline titanium dioxide electrodes. *J. Am. Chem. Soc.* **1993**, *115*, 6382-6390.
57. Kohlrausch, R. Theorie des elektrischen Rückstandes in der Leidener Flasche. *Ann. Phys.* **1854**, *167*, 56-82.
58. Williams, G.; Watts, D. C. Non-symmetrical dielectric relaxation behaviour arising from a simple empirical decay function. *Trans. Faraday Soc.* **1970**, *66*, 80-85.
59. Scher, H.; Montroll, E. W. Anomalous transit-time dispersion in amorphous solids. *Phys. Rev. B* **1975**,*12*, 2455-2477.
60. Linsey, C.P.; Patterson, G.D. The distribution of relaxation frequencies from photon correlation spectroscopy near the glass transition. *J. Chem. Phys.* **1980**, *73*, 3348 - 3354.
61. Nelson, J.; Chandler, R. E., Random walk models of charge transfer and transport in dye sensitized systems. *Coord. Chem. Rev.* **2004**, *248*, 1181-1194.
62. Nelson, J., Continuous-time random-walk model of electron transport in nanocrystalline TiO_2 electrodes. *Phys. Rev. B* **1999**, *59*, 15374-15380.
63. Cao, F.; Oskam, G.; Meyer, G.J.; Searson, P.C., Electron Transport in Porous Nanocrystalline TiO_2 Photoelectrochemical Cells. *J. Phys. Chem* **1996**, *100*, 17021-17027.
64. Hu, K.; Blair, A. D.; Piechota, E. J.; Schauer, P.A.; Sampaio, R. N.; Parlane, F.G.L.; Meyer, G. J.; Berlinguette, C. P. Kinetic pathway for interfacial electron transfer from a semiconductor to a molecule. *Nature Chem.* **2016**, *8*, 853.
65. Spettel, K. E.; Damrauer, N. H., Exploiting Conformational Dynamics of Structurally Tuned Aryl-Substituted Terpyridyl Ruthenium(II) Complexes to Inhibit Charge Recombination in Dye-Sensitized Solar Cells. *J. Phys. Chem. C* **2016**, *120*, 10815-10829.
66. Ardo, S.; Meyer, G.J. Characterization of Photoinduced Self-Exchange Reactions at Molecule–Semiconductor Interfaces by Transient Polarization Spectroscopy: Lateral Intermolecular Energy and Hole Transfer across Sensitized TiO_2 Thin Films. *J. Am. Chem. Soc.* **2011**, *133*, 15384-15396.
67. Tkaczibson, K.; Ardo, S., Numerical Monte Carlo Simulations to Evaluate the Influence that Spherical Nanoparticle Size and Arrangement has on Interparticle Charge Transport across the Surface of Dye and Cocatalyst Modified Materials. *ACS Appl. Energy Mater.* **2020**, *3*, 4699-4707.
68. Bonhôte, P.; Gognita, E.; Tingry, S.; Barbe, C.; Vlachopoulos, N.; Lenzmann, F. Comte, P.; Grätzel, M. Efficient Laterals Electron Transport inside a Monolayer of Aromatic Amines Anchored on Nanocrystalline Metal Oxide Films. *J. Phys. Chem. B* **1998**, *102*, 1498–1507
69. Moia, D.; Vaissier, V.; Lopez-Duarte, I.; Torres, T.; Nazeeruddin, M. K.; O'Regan, B. C.; Nelson, J.; Barnes, P. R. F. The reorganization energy of intermolecular hole hopping between dyes anchored to surfaces. *Chem. Sci.* **2014**, *5*, 281-290,
70. Moia, D.; Szumska, A.; Vaissier, V.; Planells, M.; Robertson, N.; O'Regan, B. C.; Nelson, J.; Barnes, P. R. F., Interdye Hole Transport Accelerates Recombination in Dye Sensitized Mesoporous Films. *J. Am. Chem. Soc.* **2016**, *138*, 13197-13206.
71. Müller, A. V.; de Oliveira, K. T.; Meyer, G. J.; Polo, A.S. Inhibiting Charge Recombination in *cis*-$Ru(NCS)_2$ Diimine Sensitizers with Aromatic Substituents. *ACS Appl. Mater.& Interfaces* **2019**, *11*, 43223-43234.

72. Sampaio, R. N.; Müller, A. V.; Polo, A. S.; Meyer, G. J. Correlation Between Charge Recombination and Lateral Hole-Hopping Kinetics in a Series of cis-Ru(phen′)(dcb)$(NCS)_2$ Dye-Sensitized Solar Cells. *ACS Applied Materials & Interfaces* **2017**, *9*, 33446-33454.
73. Clifford, J. N.; Palomares, E.; Nazeeruddin, M. K.; Grätzel, M.; Nelson, J.; Li, X.; Long, N. J.; Durrant, J. R., Molecular Control of Recombination Dynamics in Dye-Sensitized Nanocrystalline TiO_2 Films: Free Energy vs Distance Dependence. *J. Am. Chem. Soc.* **2004,** *126*, 5225-5233
74. Wang, Q.; Zakeeruddin, S. M.; Nazeeruddin, M. K.; Humphry-Baker, R.; Grätzel, M., Molecular Wiring of Nanocrystals: NCS-Enhanced Cross-Surface Charge Transfer in Self-Assembled Ru-Complex Monolayer on Mesoscopic Oxide Films. *J. Am. Chem. Soc.* **2006,** *128*, 4446-4452.
75. Sampaio, R. N.; DiMarco, B. N.; Meyer, G. J., Activation Energies for Electron Transfer from TiO_2 to Oxidized Dyes: A Surface Coverage Dependence Correlated with Lateral Hole Hopping. *ACS Energy Letters* **2017,** *2*, 2402-2407.
76. Brady, M. D.; Troian-Gautier, L.; Motley, T. C.; Turlington, M. D.; Meyer, G. J. An Insulating Al_2O_3 Overlayer Prevents Lateral Hole Hopping Across Dye-Sensitized TiO_2 Surfaces. *ACS Appl. Mater. Interfaces* **2019,** *11*, 27453-27463.
77. Hu, K.; Robson, K. C. D.; Beauvilliers, E. E.; Schott, E.; Zarate, X.; Arratia-Perez, R.; Berlinguette, C. P.; Meyer, G. J. Intramolecular and Lateral Intermolecular Hole Transfer at the Sensitized TiO_2 Interface. *J. Am. Chem. Soc.* **2014,** *136*, 1034-1046.
78. Bonhôte, P.; Moser, J.-E.; Humphry-Baker, R.; Vlachopoulos, N.; Zakeeruddin, S.M.; Walder, L.; Grätzel, M. Long-Lived Photoinduced Charge Separation and Redox-Type Photochromism on Mesoporous Oxide Films Sensitized by Molecular Dyads. *J. Am. Chem. Soc.* **1999**, *121*, 1324–1336.
79. Haque, S.A.; Handa, S.; Peter, K.; Palomares, E.; Thelakkat, M.; Durrant, J.R. Supermolecular Control of Charge Transfer in Dye-Sensitized Nanocrystalline TiO_2 Films: Towards a Quantitative Structure-Function Relationship. *Angew. Chemie Int. Ed.* **2005**, *44*, 5740-5744.
80. Argazzi, R.; Bignozzi, C. A.; Heimer, T. A.; Castellano, F. N.; Meyer, G. J. Long-Lived Photoinduced Charge Separation across Nanocrystalline TiO_2 Interfaces. *J. Am. Chem. Soc.* **1995,** *117*, 11815-11816.
81. Sherman, B. D.; Xie, Y.; Sheridan, M. V.; Wang, D.; Shaffer, D. W.; Meyer, T. J.; Concepcion, J. J. Light-Driven Water Splitting by a Covalently Linked Ruthenium-Based Chromophore–Catalyst Assembly. *ACS Energy Letters* **2016**, 124-128.
82. Brunschwig, B. S.; Sutin, N. Energy Surfaces, Reorganization Energies, and Coupling Elements in Electron Transfer. *Coord. Chem. Rev.* **1999,** *187*, 233-254.
83. Sutin, N. Theory of Electron Transfer Reactions: Insights and Hindsights. In *Progress in Inorganic Chemistry: An Appreciation of Henry Taube*, John Wiley & Sons, Inc.: Published Online, 2007; Vol. 30, pp 441-498.
84. Marcus, R. A., Electron Transfer Reactions in Chemistry. Theory and Experiment. *Rev. Mod. Phys.* **1993,** *65*, 599-610.
85. Ito, T.; Imai, N.; Yamaguchi, T.; Hamaguchi, T.; Londergan, C. H.; Kubiak, C. P., Observation and Dynamics of "Charge-Transfer Isomers". *Angew. Chem. Int. Ed.* **2004,** *43*, 1376-1381.
86. Sampaio, R. N.; Piechota, E. J.; Troian-Gautier, L.; Maurer, A. B.; Hu, K.; Schauer, P. A.; Blair, A. D.; Berlinguette, C. P.; Meyer, G. J., Kinetics teach that electronic coupling lowers the

free-energy change that accompanies electron transfer. *Proc. Natl. Acad. Sci. USA* **2018,** *115*, 7248-7253.
87. Piechota, E. J.; Troian-Gautier, L.; Sampaio, R. N.; Brennaman, M. K.; Hu, K.; Berlinguette, C. P.; Meyer, G. J., Optical Intramolecular Electron Transfer in Opposite Directions through the Same Bridge That Follows Different Pathways. *J. Am. Chem. Soc.* **2018,** *140*, 7176-7186.
88. Piechota, E. J.; Sampaio, R. N.; Troian-Gautier, L.; Maurer, A. B.; Berlinguette, C. P.; Meyer, G. J. Entropic Barriers Determine Adiabatic Electron Transfer Equilibrium. *J. Phys. Chem. C* **2019,** *123*, 3416-3425.
89. Troian-Gautier, L.; DiMarco, B. N.; Sampaio, R. N.; Marquard, S. L.; Meyer, G. J. Evidence that $\Delta S^{\ddagger}$ Controls Interfacial Electron Transfer Dynamics from Anatase TiO_2 to Molecular Acceptors. *J. Am. Chem. Soc.* **2018**, *140*, 3019-3029.
90. Ardo, S.; Sun, Y.; Staniszewski, A.; Castellano, F. N.; Meyer, G. J. Stark Effects after Excited-State Interfacial Electron Transfer at Sensitized TiO_2 Nanocrystallites. *J. Am. Chem. Soc.* **2010,** *132*, 6696-6709.
91. Cappel, U.B.; Feldt, S.M.; Schöneboom, J.; Hagfeld, A.; Boschloo, G. The Influence of Local Electric Fields on Photoinduced Absorption in Dye-Sensitized Solar Cells. *J. Am. Chem. Soc.* **2010**, *26*, 9096–9101.
92. Ward, C. L.; DiMarco, B. N.; O'Donnell, R. M.; Meyer, G. J. Dye Excited States Oriented Relative to TiO_2 Surface Electric Fields. *J. Phys. Chem. C* **2018,** *122*, 13863-13871.
93. Maurer, A. B.; Meyer, G. J., Stark Spectroscopic Evidence that a Spin Change Accompanies Light Absorption in Transition Metal Polypyridyl Complexes. *J. Am. Chem. Soc.* **2020,** *142*, 6847-6851.
94. Maurer, A. B.; Piechota, E. J.; Meyer, G. J. Excited-State Dipole Moments of Homoleptic $[Ru(bpy')_3]^{2+}$ Complexes Measured by Stark Spectroscopy. *J. Phys. Chem. A* **2019**, *123*, 8745–8754.
95. Johansson, P.G.; Kopecky A.; Galoppini, E.; Meyer, G.J. *J.* Distance Dependent Electron Transfer at TiO_2 Interfaces Sensitized with Phenylene Ethynylene Bridged Ru^{II}-Isothiocyante Compounds. *J. Am. Chem. Soc.* **2013**, *135*, 8331-8341.
96. O'Donnell, R. M.; Ardo, S.; Meyer, G. J. Charge-Screening Kinetics at Sensitized TiO_2 Interfaces. *J. Phys. Chem. Lett.* **2013,** *4*, 2817-2821.
97. Sampaio, R. N.; O'Donnell, R. M.; Barr, T. J.; Meyer, G. J., Electric Fields Control TiO_2 $(e^-) + I_3^- \rightarrow$ Charge Recombination in Dye-Sensitized Solar Cells. *J. Phys. Chem. Lett.* **2014,** *5*, 3265-3268.
98. DiMarco, B. N.; O'Donnell, R. M.; Meyer, G. J., Cation-Dependent Charge Recombination to Organic Mediators in Dye-Sensitized Solar Cells. *J. Phys. Chem. C* **2015,** *119*, 21599-21604
99. Kanemoto, K.; Takatsuki, D.; Nakatani, H.; Domoto, S. Simultaneous Monitoring of Photoinduced Absorption Signals and Short-Circuit Photocurrent during Photoexcitation in Dye-Sensitized Solar Cells. *J. Phys. Chem. C* **2017,** *121*, 12624-12630.
100. Pazoki, M.; Jacobsson, T.J.; Kullgren, J.; Johansson, E.M.J.; Hagfeldt, A.; Boschloo, G.; Edvinsson, T. Photoinduced Stark Effects and Mechanism of Ion Displacement in Perovskite Solar Cell Materials. *ACS Nano* **2017,** *11*, 2823-2834
101. Yang, W.; Vlachopoulos, N.; Boschloo, G. Impact of Local Electric Fields on Charge-Transfer Processes at the TiO_2/Dye/Electrolyte Interface. *ACS Energy Letters* **2017,** *2*, 161-167.
102. Ohta, N.; Awasthi, K.: Okoshi, K.; Manseki, K.; Miura, H.; Inoue, Y.; Nakamura, K.; Kono, H.; Diau, E.W.-G. Stark Spectroscopy of Absorption and Emission of Indoline Sensitizers:

A Correlation with the Performance of Photovoltaic Cells. *J. Phys. Chem. C* **2016,** *120*, 26206-26216.
103. Sevinc, P.C.; Dhital, B.; Rao, V.G.; Wang, Y.; Lu, H.P. Probing Electric Field Effect on Covalent Interactions at a Molecule–Semiconductor Interface. *J. Am. Chem. Soc.* **2016,** *138*, 1536-1542.
104. Idígoras, J.; Burdziński, G.; Karolczak, J.; Kubicki, J.; Oskam, G.; Anta, J.A.; Ziółek, M. The Impact of the Electrical Nature of the Metal Oxide on the Performance in Dye-Sensitized Solar Cells: New Look at Old Paradigms. *J. Phys. Chem. C* **2015,** *119*, 3931-3944.
105. Pastore, M.; De Angelis, F. Computational Modeling of Stark Effects in Organic Dye-Sensityized TiO_2 Heterointerfaces *J. Phys. Chem. Lett.* **2011,** *2*, 1261-1267.
106. DiMarco, B. N.; Troian-Gautier, L.; Sampaio, R. N.; Meyer, G. J. Dye-sensitized electron transfer from TiO_2 to oxidized triphenylamines that follows first-order kinetics. *Chem. Sci.* **2018,** *9*, 940-949.
107. Sampaio, R. N.; Li, G.; Meyer, G.J. Continuous Surface Electric Field Contraction Accompanying Electron Transfer from TiO_2 to Oxidized Sensitizers. *ACS Energy Lett.* **2016,** *1*, 846-851.
108. Sampaio, R. N.; Li, G.; Meyer, G. J. Flipping Molecules over on TiO_2 Surfaces with Light and Electric Fields. *J. Am. Chem. Soc.* **2019,** *141*, 13898-13904.
109. Scheiner, S.; Čuma, M., Relative Stability of Hydrogen and Deuterium Bonds. *J. Am. Chem. Soc.* **1996,** *118*, 1511-1521.
110. Ford, P. C.; Rudd, D. P.; Gaunder, R.; Taube, H. Synthesis and Properties of Pentaamminepyridineruthenium(II) and Related Pentaammineruthenium Complexes of Aromatic Nitrogen Heterocycles. *J. Am. Chem. Soc.* **1968,** *90*, 1187-1194.
111. Hochstrasser, R. M., Electric Field Effects on Oriented Molecules and Molecular Crystals. *Acc. Chem. Res.* **1973,** *6*, 263-269.
112. Boxer, S. G. Stark Realities. *J. Phys. Chem. B* **2009,** *113*, 2972-2983.
113. Friedrich, B.; Herschbach, D. R. Spatial Orientation of Molecules in Strong Electric Fields and Evidence for Pendular States. *Nature* **1991,** *353*, 412.
114. Block, P. A.; Bohac, E. J.; Miller, R. E. Spectroscopy of Pendular States: The Use of Molecular Complexes in Achieving Orientation. *Phys. Rev. Lett.* **1992,** *68*, 1303-1306.
115. Loesch, H. J., Orientation and Alignment in Reactive Beam Collisions: Recent Progress. *Annu. Rev. Phys. Chem* **1995,** *46*, 555-594.
116. P. P. Edwards, A. Porch, M. O. Jones, D. V. Morgan, R. M. Perks, Basic materials physics of transparent conducting oxides. *Dalt. Trans*. **2004**, 2995-3002.
117. Farnum, B. H.; Morseth, Z. A.; Lapides, A. M.; Rieth, A. J.; Hoertz, P. G.; Brennaman, M. K.; Papanikolas, J. M.; Meyer, T. J. Photoinduced Interfacial Electron Transfer within a Mesoporous Transparent Conducting Oxide Film. *J. Am. Chem. Soc.* **2014,** *136*, 2208-2211.
118. Sampaio, R. N.; Troian-Gautier, L.; Meyer, G. J. A Charge-Separated State that Lives for Almost a Second at a Conductive Metal Oxide Interface. *Angew. Chem.* **2018,** *130*, 15616-15620.
119. Farnum, B. H.; Wee, K.-R.; Meyer, T. J. Self-Assembled Molecular p/n Junctions for Applications in Dye-Sensitized Solar Energy Conversion. *Nature Chem.* **2016,** *8*, 845.
120. Wang, J. C.; Hill, S. P.; Dilbeck, T.; Ogunsolu, O. O.; Banerjee, T.; Hanson, K., Multimolecular Assemblies on High Surface Area Metal Oxides and Their Role in Interfacial Energy and Electron Transfer. *Chem. Soc. Rev.* **2018,** *47*, 104-148.

121. Lee, H.; Kepley, L. J.; Hong, H. G.; Akhter, S.; Mallouk, T. E., Adsorption of ordered zirconium phosphonate multilayer films on silicon and gold surfaces. *J. Phys. Chem* **1988,** *92*, 2597-2601.
122. Katz, H. E.; Scheller, G.; Putvinski, T. M.; Schilling, M. L.; Wilson, W. L.; Chidsey, C. E. D. Polar Orientation of Dyes in Robust Multilayers by Zirconium Phosphate-Phosphonate Interlayers. *Science* **1991,** *254*, 1485-1487.
123. Robb, A. J.; Knorr, E. S.; Watson, N.; Hanson, K., Metal ion linked multilayers on mesoporous substrates: Energy/electron transfer, photon upconversion, and more. *J. Photoch. Photobio. A* **2020,** *390*, 112291.
124. Wang, D.; Sampaio, R.N.; Troian-Gautier, L.; Farnum, B.; Sherman, B.D.; Sheridan, M.V.; Dares, C.; Marquard, S.; Meyer, G.J.; Meyer, T.J. Molecular Photoelectrode for Water Oxidation Inspired by Photosystem II. *J. Am. Chem. Soc.* **2019**, *141*, 7926-7933.
125. Bangle, R. E.; Meyer, G. J., Factors that Control the Direction of Excited-State Electron Transfer at Dye-Sensitized Oxide Interfaces. *J. Phys. Chem. C* **2019,** *123*, 25967-25976.
126. Gerischer, H.; Ekardt, W., Fermi levels in electrolytes and the absolute scale of redox potentials. *Appl. Phys. Lett* **1983,** *43* (4), 393-395.
127. Gerischer, H., *Adv. Electrochem. Electrochem. Eng.* **1961,** *1*, 139.
128. Bangle, R. E.; Schneider, J.; Piechota, E. J.; Troian-Gautier, L.; Meyer, G. J., Electron Transfer Reorganization Energies in the Electrode–Electrolyte Double Layer. *J. Am. Chem. Soc.* **2020,** *142*, 674-679
129. Bangle, R. E.; Schneider, J.; Conroy, D.T.; Aramburu-Troselj, B.M.; Meyer, G. J., Kinetic Evidence that the Solvent Barrier for Electron Transger is Absent in the Electric Double Layer. *J. Am. Chem. Soc.* **2020,** *142*, DOI: 10.1021/jacs.0c05226.
130. Finklea, H.O.; Hanshew, D.D. Electron-transfer kinetics in organized thiol monolayers with attached pentaammine(pyridine)ruthenium redox centers. *J. Am. Chem. Soc*. **1992**. *114*, 3173–3181.
131. Smalley, J. F.; Feldberg, S. W.; Chidsey, C. E. D.; Linford, M. R.; Newton, M.D.; Liu, Y.-P. The kinetics of electron transfer through ferrocene-terminated alkanethiol monolayers on gold. *J. Phys. Chem*. **1995**, *99*, 13141–13149.
132. Sumner, J. J.; Creager, S.E. Redox kinetics in monolayers on electrodes: Electron transfer is sluggish for ferrocene groups buried within the monolayer interior. *J. Phys. Chem. B*. **2001**, *105*, 8739–8745.
133. Eggers, P.K.; Darwish, N.; Paddon-Row, M. N.; Gooding, J.J. Surface-bound molecular rulers for probing the electrical double layer. *J. Am. Chem. Soc.* **2012**, *134*, 7539–7544.
134. Smalley, J.F.; Finklea, H.O.; Chidsey, C. E. D.; Linford, M.R.; Creager, S. E.; Ferraris, J. P.; Chalfant, K.; Zawodzinsk, T.; Feldberg, S. W.; Newton, M.D. Heterogeneous electron-transfer kinetics for ruthenium and ferrocene redox moieties through alkanethiol monolayers on gold. *J. Am. Chem. Soc.* **2003**, 125, 2004–2013.
135. Grahame, D.C. The electrical double layer and the theory of electrocapillarity. *Chem. Rev.* **1947**, *41*, 441–501.
136. Bockris, J.O.; Devanathan, M.A.; Müller, K. On the structure of charged interfaces. *Proc. R. Soc. London. Ser. A. Math. Phys. Sci.* **1963**, *274*, 55–79.
137. Mott, N.F.; Watts-Tobin, R.J. The interface between a metal and an electrolyte. *Electrochim. Acta.* **1961**, *79*, 79–107.
138. A. J. Bard, L. R. Faulkner, Ed., *Electrochemical Methods: Fundamentals and Applications* (John Wiley & Sons, 2nd ed., 2000).

139. Lambert, C.; Nöll, G., The Class II/III Transition in Triarylamine Redox Systems. *J. Am. Chem. Soc.* **1999,** *121*, 8434-8442.
140. Lin, B. C.; Cheng, C. P.; Lao, Z. P. M., Reorganization Energies in the Transports of Holes and Electrons in Organic Amines in Organic Electroluminescence Studied by Density Functional Theory. *J. Phys. Chem. A* **2003,** *107*, 5241-5251.
141. Biner, M.; Buergi, H. B.; Ludi, A.; Roehr, C., Crystal and molecular structures of $[Ru(bpy)_3](PF_6)_3$ and $[Ru(bpy)_3](PF_6)_2$ at 105 K. *J. Am. Chem. Soc.* **1992,** *114*, 5197-5203.
142. Marcus, R.A. On the theory of electron-transfer reactions. VI. Unified treatment for homogeneous and electrode reactions. *J. Chem. Phys*. **43**, 679–701 (1965).
143. Liu, Y. P.; Newton, M.D. Reorganization energy for electron transfer at film-modified electrode surfaces: A dielectric continuum model. *J. Phys. Chem*. **1994**, *98*, 7162–7169.
144. Ghosh, S.; Horvath, S,; Soudackov, A.V.; Hammes-Schiffer, S. Electrochemical solvent reorganization energies in the framework of the polarizable continuum model. *J. Chem. Theory Comput*. **2014**, *10*, 2091–2102.
145. Schneider, J.; Bangle, R. E.; Swords, W. B.; Troian-Gautier, L.; Meyer, G. J., Determination of Proton-Coupled Electron Transfer Reorganization Energies with Application to Water Oxidation Catalysts. *J. Am. Chem. Soc.* **2019,** *141*, 9758-9763.
146. Takeuchi, K. J.; Thompson, M. S.; Pipes, D. W.; Meyer, T. J., Redox and spectral properties of monooxo polypyridyl complexes of ruthenium and osmium in aqueous media. *Inorg. Chem.* **1984,** *23*, 1845-1851.
147. Trammell, S. A.; Wimbish, J. C.; Odobel, F.; Gallagher, L. A.; Narula, P. M.; Meyer, T. J., Mechanisms of Surface Electron Transfer. Proton-Coupled Electron Transfer. *J. Am. Chem. Soc.* **1998,** *120*, 13248-13249.
148. Ghosh, S.; Horvath, S,; Soudackov, A.V.; Hammes-Schiffer, S. Electrochemical electron transfer and proton-coupled electron transfer: Effects of double layer and ionic environment on solvent reorganization energies. *J. Chem. Theory Comput*. **2016**, *12*, 2917–2925.
149. https://www.nrel.gov/pv/cell-efficiency.html
150. Huaulmé, Q.; Mwalukuku, V.M..; Joly, D.; Liotier, J.; Kervella, Y.; Maldivi, P.; Narbey, S.; Oswald, F.; Riquelme, A.J.; Anta, J.A.; Demadrille, R.. Photochromic dye-sensitized solar cells with light-driven adjustable optical transmission and power conversion efficiency. *Nature Energy* **2020**, *5*, 468–477.
151. Freitag, M.; Teuscher, D. J.; Saygili, Y.; Zhang, D. X.; Giordano, D. F.; Liska, D. P.; Hua, P. J.; Zakeeruddin, S. M.; Moser, J.-E.; Grätzel, M.; Hagfeldt, A. Dye-Sensitized Solar Cell for Efficient Power Generation under Ambient Lighting. *Nat. Photonics* **2017**, *11*, 372-378.
152. Michaels. H.; Rinderle. M.; Freitag. R.; Benesperi. I.; Edvinsson. T.; Socher. R.; Gagliardi. A.; Freitag, M. Dye-sensitized solar cells under ambient light powering machine learning: towards autonomous smart sensors for the internet of things. *Chem. Sci.* **2020**, *11*, 2895–2906.
153. Aghazada, S.; Gao, P.; Yella, A.; Marotta, G.; Moehl, T.; Teuscher, J.; Moser, J.-E.; De Angelis, F.; Grätzel, M.; Nazeeruddin, M.K. Ligand Engineering for the Efficient Dye-Sensitized Solar Cells with Ruthenium Sensitizers and Cobalt Electrolytes. *Inorg. Chem.* **2016,** *55*, 6653-6659.
154. Gao, J.; Prajapati, G.K.; Hao, Y.; Kloo, L. Exploring Lewis-Base Effects to Improve the Efficiency of $[Co(bpy)_3]^{2+/3+}$-Mediated Dye-Sensitized Solar Cells. *ACS Appl. Energy Mater*. **2020**, *3*, 5705–5711.

155. Ogunsolu, O.O.; Braun, A.J.; Robb, A.J.; Salpage, S.R.; Zhou, Y.; Hanson, K. Influence of Dye-Coordinated Metal Ions on Electron Transfer Dynamics at Dye–Semiconductor Interfaces. *ACS Applied Energy Mater.* **2019**, *2*, 29-36.
156. Dragonetti, C.; Magni, M.; Colombo, A.; Melchiorre, F.; Biagini, P.; Roberto, D. Coupling of a Copper Dye with a Copper Electrolyte: A Fascinating Springboard for Sustainable Dye-Sensitized Solar Cells. *ACS Applied Energy Mater.* **2018**, *1*, 751-756.
157. Glinka, A.; Gierszewski, M.; Gierczyk, B.; Burdziński, G.; Michaels, H.; Freitag, M.; Ziółek, M. Interface Modification and Exceptionally Fast Regeneration in Copper Mediated Solar Cells Sensitized with Indoline Dyes. *J. Phys. Chem. C* **2020**, *124*, 2895–2906.
158. Leandri, V.; Pizzichetti, A. R. P.; Xu, B.; Franchi, D.; Zhang, W.; Benesperi, I.; Freitag, M.; Sun, L.; Kloo, L.; Gardner, J. M. Exploring the Optical and Electrochemical Properties of Homoleptic versus Heteroleptic Diimine Copper(I) Complexes. *Inorg. Chem.* **2019**, *58*, 12167–12177.
159. Saygili, Y.; Stojanovic, M.; Michaels, H.; Tiepelt, J.; Teuscher, J.; Massaro, A.; Pavone, M.; Giordano, F.; Zakeeruddin, S.M.; Boschloo, G.; Moser, J.-E.; Grätzel, M.; Muñoz-García, A.B.; Hagfeldt, A.; Freitag, M. Effect of Coordination Sphere Geometry of Copper Redox Mediators on Regeneration and Recombination Behavior in Dye-Sensitized Solar Cell Applications. *ACS Applied Energy Mater.* **2018**, *1*, 4950-4962.
160. Saygili, Y.; Stojanovic, M.; Kim, H.-S.; Teuscher, J.; Scopelliti, R.; Freitag, M.; Zakeeruddin, S. M.; Moser, J.-E.; Grätzel, M.; Hagfeldt, A. Liquid State and Zombie Dye Sensitized Solar Cells with Copper Bipyridine Complexes Functionalized with Alkoxy Groups. *J. Phys. Chem. C* **2020,** *124*, **7071-7081.**
161. Kessinger, M.C.; Langlois, R.; Roof, J.; Shaikh, S.M.; Tanko, J.M.; Morris, A.J. Improving the Efficiency of the $Mn^{2+/3+}$ Couple in Quantum Dot Solar Cells: The Role of Spin Crossover. *J. Phys. Chem. C* **2018**, *122*, 14135-14149.
162. Ruess, R.; Horn, J.; Ringleb, A.; Schlettwein, D. Efficient Electron Collection by Electrodeposited ZnO in Dye-Sensitized Solar Cells with $TEMPO^{+/0}$ as the Redox Mediator. *J. Phs. Chem. C* **2019,** *123*, 22074-22082.
163. Li, B.; Wang, L. Kang, B.; Wang, P.; Qiu, Y. Review of recent progress in solid-state dye-sensitized solar cells. *Solar Energy Mater. Solar Cells* **2006**, *90*, 549-573.
164. Moia, D.; Leijtens, T.; Noel, N.; Snaith, H. J.; Nelson, J.; Barnes, P. R. F. Dye Monolayers Used as the Hole Transporting Medium in Dye-Sensitized Solar Cells. *Adv. Mater.* **2015**, *27*, 5889-5894.
165. Fujishima, A.; Honda, K. Electrochemical photolysis of water at a semiconducting electrode. *Nature* **1972**, *238*, 37-38.
166. Oshima, T.; Nishioka, S.; Kikuchi, Y.; Hirai, S.; Yanagisawa, K.-I.; Eguchi, M.; Miseki, Y.; Yui, T.; Kimoto, K.; Sayama, K.; Ishitani, O.; Mallouk, T.E.; Maeda, K. An artificial Z-scheme constructed from dye-sensitized metal oxide nanosheets for visible light-driven overall water splitting. *J. Am. Chem. Soc.* **2020**, *142*, 8412–8420.
167. Sheridan, M. V; Wang, Y.; Wang, D.; Troian-Gautier, L.; Dares, C. J.; Sherman, B. D.; Meyer, T. J. Light-Driven Water Splitting Mediated by Photogenerated Bromine. *Angew. Chemie Int. Ed.* **2018**, *57*, 3449–3453.
168. Swierk, J. R.; Mallouk, T. E. Design and development of photoanodes for water-splitting dye-sensitized photoelectrochemical cells. *Chem. Soc. Rev.* **2013**, *42*, 2357–2387.
169. Berardi, S.; Drouet, S.; Francas, L.; Gimbert-Surinach, C.; Guttentag, M.; Richmond, C.; Stoll, T.; Llobet, A. Molecular Artifical Photosynthesis. *Chem. Soc. Rev.* **2014**, *43*, 7501–7519.

170. Brennaman, M. K.; Dillon, R. J.; Alibabaei, L.; Gish, M. K.; Dares, C. J.; Ashford, D. L.; House, R. L.; Meyer, G. J.; Papanikolas, J. M.; Meyer, T. J. Finding the Way to Soalr Fuels with Dye-Sensitized Photoelctrosynthesis Cells. *J. Am. Chem. Soc.* **2016**, *138*, 13085–13102.
171. Zhang, B.; Sun, L. Artificial Photosynthesis: Opportunities and Challenges of Molecular Catalysts. *Chem. Soc. Rev.* **2019**, *48,* 2216-2264.
172. Wong, D.-I.; Lee, J.-S.; Ji. J.-M.; Son, H.-J.; Pac, C.; Kang, S.O. Highly Robust Hybrid Photocatalyst for Carbon Dioxide Reduction: Tuning and Optimization of Catalytic Activities of Dye/TiO_2/Re(I) Organic-Inorganic Ternary Systems. *J. Am. Chem. Soc.* **2015**, *137*, 13679-13690.
173. Ardo, S.; Achey, D.; Morris, A.J.; Abrahamsson, M.; Meyer, G.J. Non-Nernstian Two-Electron Transfer Photocatalysis at Metalloporphyrin–TiO_2 Interfaces. *J. Am. Chem. Soc.* **2011**, *133*, 16572-16580.
174. Obare, S.O.; Ito, T.; Meyer, G.J. Multi-electron Transfer from Heme Functionalized Nanocrystalline TiO_2 to Trichlororethylene. *J. Am. Chem. Soc.* **2006**, *128*, 712-713.
175. Griller, D.; Ingold, K.U. Free-radical clocks. *Acc. Chem. Res*. **1980**, *13*, 317–323.
176. Stromberg, J.R.; Wnuk, J.; Pinlac, R.A.F.; Meyer, G.J. Multi-electron Transfer at Heme Functionalized Nanocrystalline TiO_2: Reductive Dechlorination of DDT and CCl_4 forms Stable Carbene Compounds. *Nano Lett.* **2006**, *6,* 1284-1286.
177. Schrauben, J.N.; Hayoun, R.; Valdez, C.N.; Braten, M.; Fridley, L.; Mayer, J.M. Titanium and Zinc Oxide Nanoparticles are Proton-Coupled Electron Transfer Agents. *Science* **2012**, *336*, 1298-1301.
178. Schimpf, A.M.; Lounis, S.D.; Runnerstrom, E.L.; Milliron, D.J.; Gamelin, D.R. Redox Chemistries and Plasmon Energies of Photodoped In_2O3 and Sn-Doped In_2O_3 (ITO) Nanocrystals *J. Am. Chem. Soc.* **2015**, *137*, 518–524.
179. Ramesha, G.K.; Brennecke, J.F.; Kamat, P.V. Origin of Catalytic Effect in the Reduction of CO_2 at Nanostructured TiO_2 Films *ACS Catal.* **2014**, *4*, 3249–3254.
180. Schwarz, H.; Shaik, S.; Li, J. Electronic Effects on Room-Temperature, Gas-Phase C–H Bond Activations by Cluster Oxides and Metal Carbides: The Methane Challenge. *J. Am. Chem. Soc.* **2017**, *139*,17201–17212.
181. Shaw, M.H.; Twilton, J.; MacMillan, D.W.C. Photoredox Catalysis in Organic Chemistry *J. Org. Chem.* **2016**, *81*, 6898–6926.
182. Romero, N.A.; Nicewicz, D.A. Organic Photoredox Catalysis. *Chem. Rev.* **2016**, *116,* 10075–10166.
183. Wang, C.-S.; Dixneuf, P.H.; Soulé, J.-F. Photoredox Catalysis for Building C–C Bonds from C(sp2)–H Bonds. *Chem. Rev.* **2018**, *118*, 7532–7585.
184. Dongare, P.; MacKenzie, I.; Wang, D.; Nicewicz, D. A.; Meyer, T. J. Oxidation of Alkyl Benzenes by a Flavin Photooxidation Catalyst on Nanostructured Metal-Oxide Films. *Proc. Natl. Acad. Sci. U.S.A.* **2017**, *114*, 9279-9283.

For TOC use only